RESEARCH ARTICLE

Morphology and Connectivity of Parabrachial and Cortical Inputs to Gustatory Thalamus in Rats

Stephen L. Holtz, Anqi Fu, Wyatt Loflin, James A. Corson, and Alev Erisir*

[1]Department of Psychology, University of Virginia, Charlottesville Virginia 22904-4400

ABSTRACT

The ventroposterior medialis parvocellularis (VPMpc) nucleus of the thalamus, the thalamic relay nucleus for gustatory sensation, receives primary input from the parabrachial nucleus, and projects to the insular cortex. To reveal the unique properties of the gustatory thalamus in comparison with archetypical sensory relay nuclei, this study examines the morphology of synaptic circuitry in the VPMpc, focusing on parabrachiothalamic driver input and corticothalamic feedback. Anterogradely visualized parabrachiothalamic fibers in the VPMpc bear large swellings. At electron microscope resolution, parabrachiothalamic axons are myelinated and make large boutons, forming multiple asymmetric, adherent, and perforated synapses onto large-caliber dendrites and dendrite initial segments. Labeled boutons contain dense-core vesicles, and they resemble a population of terminals within the VPMpc containing calcitonin gene-related peptide. As is typical of primary inputs to other thalamic nuclei, parabrachiothalamic terminals are over five times larger than other inputs, while constituting only 2% of all synapses. Glomeruli and triadic arrangements, characteristic features of other sensory thalamic nuclei, are not encountered. As revealed by anterograde tracer injections into the insular cortex, corticothalamic projections in the VPMpc form a dense network of fine fibers bearing small boutons. Corticothalamic terminals within the VPMpc were also observed to synapse on cells that were retrogradely filled from the same injections. The results constitute an initial survey describing unique anatomical properties of the rodent gustatory thalamus. J. Comp. Neurol. 523:139–161, 2015.

INDEXING TERMS: ventroposteromedial thalamus; cortical feedback; CGRP; electron microscopy; 3D reconstruction; RGD_70508; AB_2336827; AB_259000; AB_2336171; rid_000042; nif-0000–23420; nlx_152120

The chemical identities of taste stimuli and the psychological aspects of orosensory experience, such as palatability and expectation, collectively influence information processing in the rodent gustatory cortex (Katz et al., 2001; Spector and Travers, 2005; Stapleton et al., 2006; Carleton et al., 2010; Samuelsen et al., 2012). Taste information reaches the gustatory cortex from two pathways: a thalamocortical projection from the venteroposterior medialis parvocellularis nucleus of the thalamus (VPMpc; Kosar et al., 1986a), and limbic projections, including those from the lateral hypothalamus and amygdala (Norgren, 1976; Allen et al., 1991). These inputs are distinct in terms of the cortical areas they target and their function. Projections directly from limbic structures tend to be more diffuse within the insular cortex (Allen et al., 1991), and are implicated in affective aspects of gustatory processing (Piette et al., 2012; Samuelsen et al., 2012). In contrast, thalamocortical projections from the VPMpc largely terminate in the granular and dysgranular insular cortex, and provide orosensory aspects of taste processing (Sewards, 2004; Samuelsen et al., 2013). Similar to the role of thalamic relay nuclei in other systems (Malpeli, 1983; Poulet et al., 2012), blockade of neuronal activity in the VPMpc hampers the ability of the cortex to process gustatory information (Samuelsen et al., 2013). Despite its importance in the hierarchy of information flow, our knowledge of the synaptic circuitry of the gustatory thalamus remains rudimentary.

Grant sponsor: National Institute on Deafness and Communication Disorders, National Institutes of Health; Grant number: R01DC10183 (to A.E.); Grant sponsor: University of Virginia Double-Hoo Award (to S.L.H. and J.A.C.).

Dr. Corson's present address is: School of Dentistry, University of Michigan, 1011 N. University Ave., Ann Arbor, MI 48109. E-mail: jcorson@umich.edu

*CORRESPONDENCE TO: Alev Erisir, Department of Psychology, University of Virginia, PO Box 400400, Charlottesville, VA 22904. E-mail: erisir@virginia.edu

Received January 6, 2014; Revised August 24, 2014;
Accepted August 27, 2014.
DOI 10.1002/cne.23673
Published online September 4, 2014 in Wiley Online Library (wileyonlinelibrary.com)

In the rat gustatory system, taste information from the oral cavity travels through the nucleus of the solitary tract (NTS), and then to the parabrachial nucleus of the pons (PBN) before reaching the VPMpc (Blum et al., 1943; Benjamin and Akert, 1959; Emmers, 1964; Norgren and Leonard, 1971, 1973; Hamilton and Norgren, 1984; Pritchard et al., 1986; Herbert et al., 1990). PBN input to the VPMpc arises primarily from the gustatory-responsive, waist region of the ipsilateral PBN (Lasiter and Kachele, 1988; Halsell and Travers, 1997; Karimnamazi and Travers, 1998; Krout and Loewy, 2000; Tokita et al., 2010). Presumed relay cells of the VPMpc send thalamocortical axons to the insular cortex (Norgren and Wolf, 1975; Kosar et al., 1986a; Allen et al., 1991), which is reciprocally connected to the VPMpc (Kosar et al., 1986b). The VPMpc also projects to the thalamic reticular nucleus (TRN; Stehberg et al., 2001), probably via axon collaterals of thalamocortical relay cells. The TRN sends inhibitory projections back to the VPMpc (Hayama et al., 1994; Hanamori, 2003), forming an intrathalamic feedback loop.

To describe the morphological properties of putative taste axons originating in the PBN and projecting to the VPMpc (henceforth referred to as parabrachiothalamic terminals) at electron microscope resolution, the present study utilized tract tracing to fill axons anterogradely from the PBN waist region, which was considered to contain neurons responsive to taste stimuli. Corticothalamic axons were studied after anterograde tracer injections into the insular cortex. Terminals from both areas were examined under the light microscope for localization within the the VPMpc and under the electron microscope for quantitative ultrastructural analysis.

MATERIALS AND METHODS

Animals

A total of 25 adult female Sprague–Dawley rats (Harlan, Houston, TX; RRID:RGD_70508) were used. Fourteen animals received tracer injections in the PBN, six received tracer injections in the insular cortex (IC), two received injections into the VPMpc, and three received no injection, but were processed for calcitonin gene-related peptide (CGRP) immunoreactivity. Four PBN-injection, and three IC-injection brains, in which the injection site was the PBN or IC, and with acceptable structural preservation, were processed for electron microscopy. All animals were maintained on a 12:12-hour light:dark cycle and had *ad libitum a*ccess to water and standard rat feed. Rats were 3–6 months old, and weighed less than 250 g at the time of injections. All procedures were approved by the University of Virginia Institutional Animal Care and Use Committee.

Tracer injections

Animals were anesthetized with a combination of ketamine (75 mg/kg i.p.) and medetomidine (0.5 mg/kg i.p.), and placed into a nontraumatic stereotaxic apparatus (Kopf, Tujunga, CA). The skull was exposed to reveal bregma, lambda, and sagittal sutures, and a small hole was drilled. For PBN injections, the craniotomy was centered 11.4 mm caudal to bregma and 1.7 mm lateral to the midsagittal suture. PBN injections were angled caudal to rostral at 20° and descended 5.5 mm from the dural surface. VPMpc injections were 4.45 mm caudal to bregma, and 1.1 mm lateral to the midsagittal suture; injections descended perpendicular to the skull 6.6 mm from the dural surface.

For IC injections, a lateral craniotomy was performed to expose the intersection of the rhinal vein and medial cerebral artery. Three injections were made 2 mm dorsal to this intersection and a along a strip 2 mm anterior (one site) and posterior (two injection sites) to the medial cerebral artery. A glass pipette filled with tracer was lowered 1–2 mm perpendicular to the cortex surface. Approximately 200 nl of biotinylated dextran amine (BDA; Invitrogen, Carlsbad, CA) in acidic medium (citrate buffer; pH 3.0) or neutral medium was injected

Abbreviations

3V	third ventricle
4V	fourth ventricle
AI	agranular insular cortex
CGPn	central gray of the pons
CGRP	calcitonin gene-related peptide
Cp	cerebral peduncle
CPu	caudate/putamen
CT	corticothalamic
DI	dysgranular insular cortex
Ec	external capsule
el	external lateral parabrachial nucleus
em	external medial parabrachial nucleus
f	fornix
fr	fasciculus retroflexus
GI	granular insular cortex
IC	insular cortex
ic	internal capsule
m	medial parabrachial nucleus
Me5	mesencephalic trigeminal nucleus
me5	mesencephalic trigeminal tract
ml	medial lemniscus
mt	mammillothalamic tract
NTS	nucleus tractus solitarii
PBN	parabrachial nucleus
PT	parabrachiothalamic
scp	superior cerebellar peduncle
sp5	spinal trigeminal tract
spf	subparafascicular thalamic nucleus
TRN	thalamic reticular nucleus
vl	ventral lateral parabrachial nucleus
VPM	ventral posteromedial thalamic nucleus
VPMpc	ventroposterior medialis parvocellularis nucleus
w	waist region of the parabrachial nucleus.

TABLE 1.
Antibodies Used in This Study

Name	Host	Antigen characteristics	Source	Dilution
Anti-calcitonin gene-related peptide antibody	Mouse (monoclonal)	C-terminal 10 amino acids of rat CGRP (Wong et al. 1993)	Sigma Aldrich, St. Louis, MO, cat. no. C7113 RRID:AB_259000	1:1,000
Anti-mouse secondary antibody	Goat (polyclonal)	Mouse IgG, conjugated to biotin	Vector, Burlingame, CA, cat. no. BA-9200 RRID:AB_2336171	1:100

by using a glass micropipette with fine inner lumen (0.25 mm; A-M Systems, Carlsborg, WA) and a Picospritzer III (Parker Hannifin, Cleveland, OH) at each site. As acidic medium allows BDA to travel both anterogradely and retrogradely, it was used for both PBN and VPMpc injections, which provided confirmation of input from the NST and PBN, respectively. Nonacidic medium that facilitates transport in fine axons was used to study feedback projections in IC injections (Reiner et al., 2000), although these also led to retrograde labeling in the thalamus. The volume of tracer injected was calculated based on the inner diameter of the pipette and the advance of the tracer fill-line that was plunged after small air puffs applied through the pipette.

Following injections, the scalp was sutured, and the animal was revived with atipamezole (1 mg/kg) and administered the postoperative analgesic buprenex (3 mg/kg). Following a 3-day survival time, the animal was deeply anesthetized with an overdose of Nembutal (excess of 150 mg/kg i.p.) and transcardially perfused using room-temperature Tyrode's solution (137 mM NaCl, 5.5 mM dextrose/glucose, 1.2 mM $MgCl_2$, 2 mM KCl, 0.4 mM NaH_2PO_4, 0.9 mM $CaCl_2$, 11.9 mM $NaHCO_3$, in 1 L filtered dH_20) followed by 4% paraformaldehyde in 0.1 M phosphate buffer (PB; pH 7.4) for light microscopy–processed animals. An additional 0.5% glutaraldehyde was added to the paraformaldehyde for animals used for electron microscopy. Brains were removed and allowed to postfix overnight in 4% paraformaldehyde at room temperature before blocking and sectioning of the brainstem and thalamus in 60-μm coronal sections on a vibratome. Sections that were not processed immediately were treated with 1% sodium borohydrate in PB to stop fixation and stored in 0.05% sodium azide in PBS at 4°C.

Tissue preparation

Sections for light microscopy were processed serially in three interleaved sets to view the tracer localization relative to histochemical markers. The first series was permeabilized with 0.1% Triton X-100 in phosphate-buffered saline (PBS) for 30 minutes, and incubated in a 1:100 dilution of avidin–biotin peroxidase (ABC kit; Vector, Burlingame, CA, cat. no. PK-7100, RRID:AB_2336827) overnight at 4°C. Tracer-containing neuropil was visualized with diaminobenzidine (DAB). The second series was stained with Cresyl Violet for cell body visualization. The third series was treated with gold hydrochloride, to view myelination, as described previously (Corson et al., 2012).

Briefly, sections mounted onto gelatin-subbed slides were rehydrated in 0.01 M PBS for 2 minutes and then incubated in 0.1% $HAuCl_4$ in 0.02 M PBS (pH 7.0) for 10–12 minutes at 60°C. After fine myelination was differentiated, the slides were incubated in 0.1% $KAuCl_4$ in saline (pH 7.0) for 3 minutes at 60°C. Following 2× 2-minute rinses in 0.01 M PBS, the slides were incubated in 1% sodium thiosulfate in dH_2O at 60°C for 3 minutes, rinsed 5× 3 minutes in 0.01 M PBS, dehydrated, and coverslipped. These series allowed identification of anterogradely labeled terminal locations in histologically defined nuclei. All sections were mounted serially on gelatin-subbed slides, dehydrated, and coverslipped with DPX mounting media (Sigma Aldrich, St. Louis, MO).

Sections for electron microscopy were processed with DAB as above, and embedded in plastic resin using standard procedures. Briefly, the sections were postfixed with 4% osmium tetroxide for 1 hour, counterstained with uranyl acetate (in 70% ETOH), dehydrated in increasing concentrations of ETOH, followed by treatments in acetone, an acetone and resin mixture, and pure resin. Sections were flat-embedded between two sheets of Aclar Embedding Film (Electron Microscopy Sciences, Warrington, PA) and polymerized at 60°C for 24–48 hours, before re-embedding of sections containing the VPMpc in capsules for ultrathin sectioning. Capsules were trimmed, and 70-nm sections were cut by using an ultramicrotome (Leica, Deerfield, IL, model EM UC7) at planes quasi-parallel to the surface to obtain uniformly labeled trapezoids. In all brains, labeling was found to have penetrated well into the embedded sections, allowing for several rounds of ultrathin sectioning with sufficient label per block face. Copper mesh grids

were used for general circuitry analysis, and copper slot grids (Electron Microscopy Sciences) were used for 3D reconstruction.

Tissue sections used for CGRP immunostaining were first treated with 1% sodium borohydrate for 30 minutes, rinsed in 0.01 M PBS until the bubbles had cleared, and then blocked in 1% bovine serum albumin (BSA; Sigma Aldrich) in 0.01 M PBS for 30 minutes. The sections were then incubated in a monoclonal antibody against CGRP (Sigma-Aldrich, cat. no. C7113, RRID:AB_259000; 1:1000; Table 1) and 1% BSA in 0.01 M PBS with 0.05% NaN_3 and 0.06% Triton X-100 (ICN Biomedicals, Costa Mesa, CA) for 1–3 days. The CGRP antibody (clone #4901) was produced monoclonally against a 10-polypeptide sequence (out of 37) of rat CGRP, recognizing both CGRP-I and CGRP-II (Wong et al., 2014). The sensitivity and specificity to rat CGRP were characterized by radioimmunoassay. The #4901 antibody completely abolished the portal release of somatostatin and the inhibition of gastric acid secretion induced by intravenous infusion of rat CGRP in anesthetized rats (Wong et al., 2014). This antibody lacks positive immunoreactivity in histological sections from α-CGRP knockouts (Zhang et al., 2001). The pattern of CGRP immunoreactivity detected in the current study was also in agreement with previous studies of CGRP immunoreactivity using other antibodies (Yasui et al., 1989, 1991). The sections were then rinsed in 0.01 M PBS to terminate the primary incubation, and transferred into biotinylated anti-mouse secondary antibody (Vector, cat. no. BA-9200 RRID:AB_2336171; 1:100 dilution) for 2 hours, followed by ABC-DAB visualization.

Analysis and statistics

Mounted sections were analyzed and photographed by using a Leica DC100 digital camera mounted on a Leica light microscope (model LMDC 888011). All images were captured at a resolution to discern single fibers (myelin or tracer labeled) using 40× or 63× objectives. Large fields of view, to capture full coronal sections, were created by tiling adjacent images using Adobe (San Jose, CA) Photoshop CS5 software. For selecting areas to be analyzed on the electron microscope, resin-embedded sections, adjacent to myelin- and Nissl-labeled mounted slides, were also imaged on the light microscope. Special care was taken to correctly document anatomical landmarks, such as the mammillothalamic tract, medial lemniscus, fasciculus retroflexus, habenular nucleus, and fornix to ensure accurate sampling from within the VPMpc for electron microscopy. Once the landmarks of tissue were identified on the resin-embedded sections, blocks were trimmed to contain the VPMpc, and 80-nm ultrathin sections were cut on a Leica Ultracut UTC7 from the surface 2–5 μm of the blocks containing immunolabel. Electron micrographs were taken with a JEOL (Peabody, MA) 1010 transmission electron microscope equipped with a 16-megapixel CCD camera.

For synapse density analysis, edge-overlapped images were taken at 10,000× magnification to make composite pictures of large regions within the VPMpc, along a 30–50 μm strip of tissue at the tissue–resin interface. The composite areas contained 666 synapses in total. This dataset was used for analysis of labeled terminal frequency. For quantification of labeled terminal morphology, a second dataset (comprised of images of all labeled instances encountered in ultrathin sections) was captured. The pixel resolution of the electron microscopy images was 2.75 nm. Image ProPlus 5.1 (Media Cybernetics, Silver Spring, MD) was used to make measurements from micrographs. Data analysis was completed by using Microsoft Excel 2007 and SPSS (RRID:rid_000042); graphs and figures were created with OriginPro 7.5, Adobe Photoshop CS5, and Adobe Illustrator CS5. Three-dimensional reconstructions were completed by using the software Synapse Web Reconstruct (Fiala, 2005; RRID:nif-0000–23420).

To estimate dendrite calibers, the "feret minimum" ($feret_{min}$) measure of Image ProPlus (Media Cybernetics) was used. This algorithm optimally places a rectangle outside the dendrite cross-sectional outline, the shape of which may vary from round to elliptical (at bifurcation points more irregular cross sections form). Whereas the long side of this rectangle ($feret_{max}$) depends on how obliquely the cylindrical dendrite was cut, the short side ($feret_{min}$) provides a close estimate of the cylinder caliber. Please note that "$feret_{min}$" is different from the "shortest diameter" measurement that is occasionally used in the literature in that $feret_{min}$ is not affected by irregularities in dendrite shape, or the relative position of the longitudinal cut-plane to the axis of the cylinder. With the exception of the unlikely instances in which a dendrite may be sectioned at the apex of a bend, $feret_{min}$ measurements are the most accurate estimate of the caliber of a cylindrical dendrite using 2D cross sections. For terminal area measurements, labeled and unlabeled terminals were outlined; for synapse density analysis, each synapse was counted, and its cross-sectional length and the small neuropil area (area within each image excluding blood vessels, somata, and myelinated axons) were measured. Nonparametric statistical tools were used for comparisons of area measures obtained from terminal or dendrite populations.

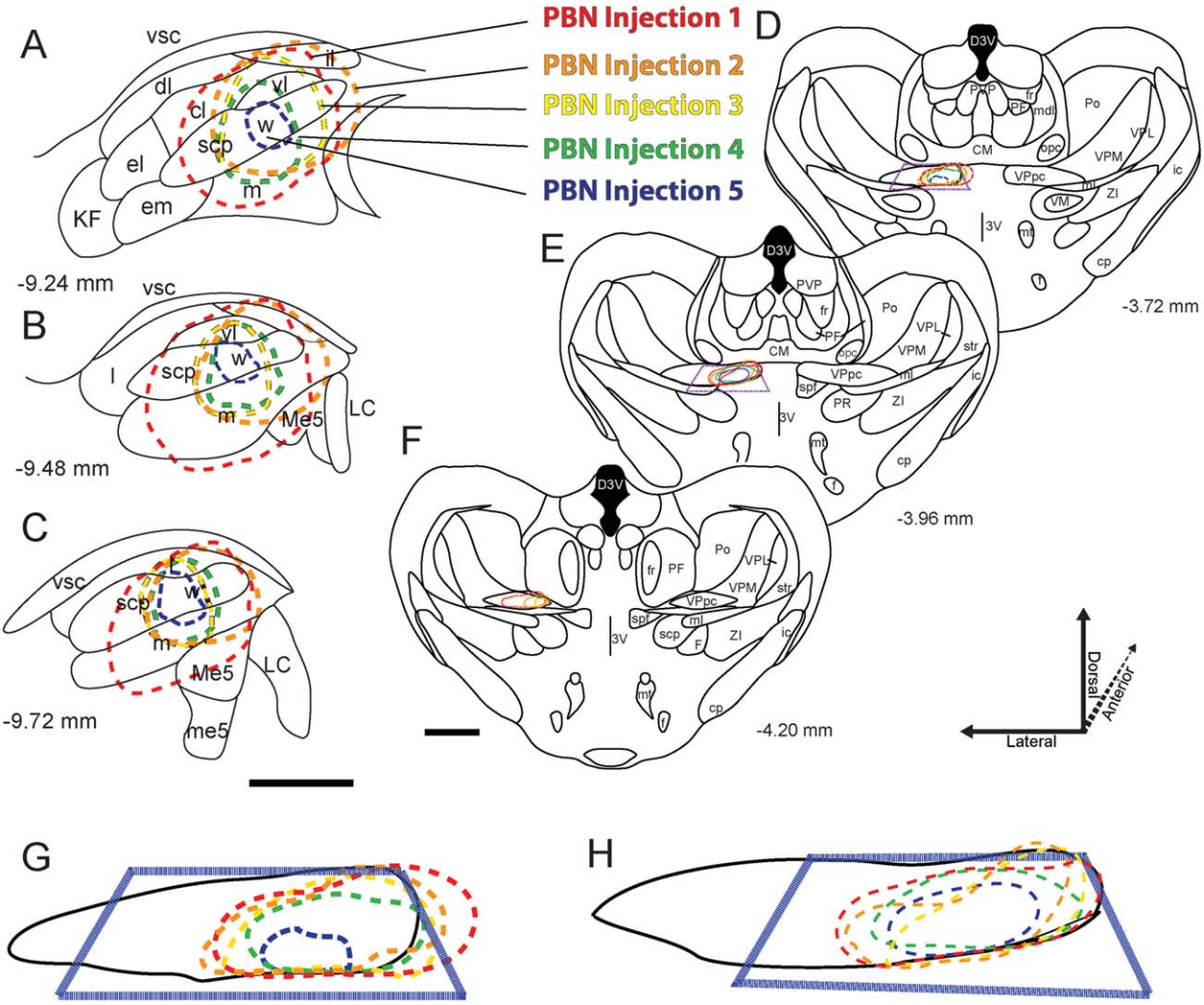

Figure 1. Tracer injections sites in the parabrachial nucleus (PBN) (**A–C**) and corresponding projection sites in the thalamus (**D–F**). Each color-coded dashed line outlines the densest region of tracer labeling in the brainstem in coronal sections corresponding to stereotaxic coordinates AP-9.24 (A), AP-9.48 (B), and AP-9.72 (bregma; Paxinos Rat Atlas); these are marked as PBN injections 1–5 (A). For each injection, the projection site in the thalamus is also marked in corresponding coronal sections from the Paxinos Rat Atlas, at AP-3.72, AP-3.96, and AP-4.20 (D–F). **G,H:** Close-up images of the VPMpc (black outline) of each coronal section illustrated in D and E, redrawn to illustrate the borders of densest projection from each injection in the thalamus. The blue trapezoid represents the region that was prepared for electron microscopy analysis in cases PBN injections 2–5. For abbreviations, see list. Scale bar = 0.6 mm in C (applies to A–C); 1 mm in F (applies to D–F).

RESULTS

Parabrachiothalamic input to the VPMpc

Light microscopy

Stereotaxic injections of BDA into the gustatory responsive waist region of the parabrachial nucleus led to visualization of parabrachiothalamic axons in the ipsilateral medial thalamus, with a particularly dense projection site situated dorsal and medial to the medial lemniscus (Figs. 1, 2). By using serial coronal sections processed for DAB (tracer), Nissl, or myelin in sequence, the region of dense projections was transposed onto adjacent Nissl- and myelin-stained sections, using the medial lemniscus (ml) and blood vessels as landmark structures (Fig. 2D–K). Next, the Nissl–DAB–myelin triplets were matched to comparable sections from a digital rat brain atlas (Paxinos and Watson, 2007; Rat Brain Atlas of Paxinos and Watson, RRID:nlx_152120), based on the outlines of the ic, cp, habenula, ml, mt, and f (Fig. 2G,K).

As outlined in the Rat Brain Atlas, the VPMpc extended approximately 1 mm in the medial–lateral axis, and 0.8 mm in the anterior–posterior axis.

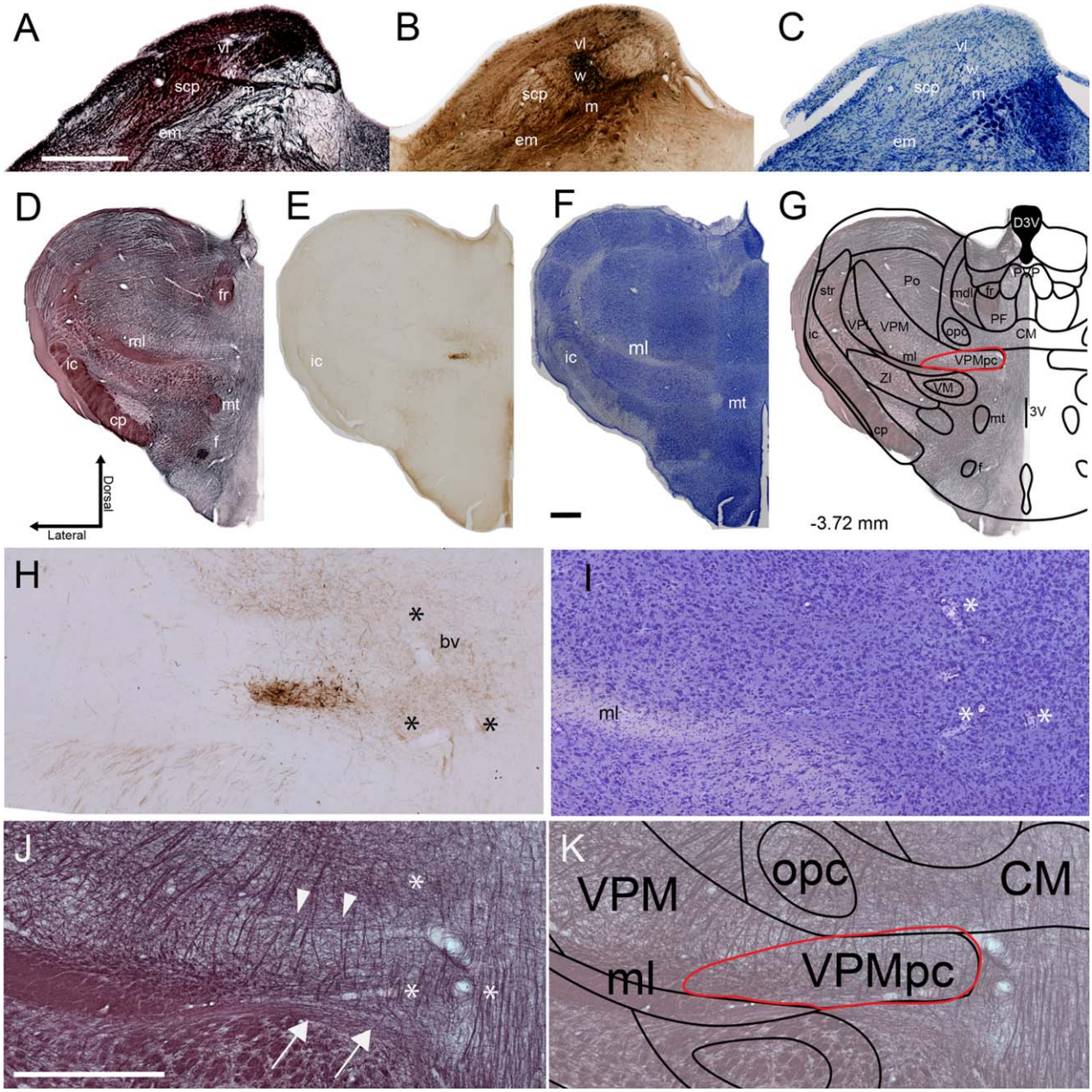

Figure 2. Tracer injection site in a representative coronal section of the parabrachial nucleus (this case is illustrated as PBN injection 5 in Fig. 1). Adjacent sections that represented the core of the injection site were stained for myelin (**A**), for tracer (**B**), and for Nissl (**C**). Section in B corresponds to −9.48 mm AP coordinates (from bregma). The core of the tracer injection site (B) was confined in the waist region (w) of the PBN. Both Nissl- and DAB-stained sections were useful in identifying the nucleus borders (dashed lines in C). Myelin (**D,J**), tracer (**E,H**), and Nissl (**F,I**) stained adjacent sections through the thalamus, containing anterograde tracer projection site in the VPMpc. The asterisks mark blood vessel (bv) landmarks that appeared in adjacent myelin/DAB/Nissl sections. Overlay of the corresponding section from the Paxinos Rat Brain Atlas (**G,K**) marks presumed borders of the VPMpc (red outline). Neither myelin nor Nissl stain outline a discernable border around the VPMpc, although mediolaterally coursing myelinated axons (white arrowheads in J) corresponded to the dorsal border of the VPMpc. Myelin stain clearly demarcates the medial lemniscus (ml), which outlines the VPMpc ventrally and tapers down about the midpoint of the mediolateral dimension of the VPmpc. Also, an additional fiber bundle (white arrows in J), represents a local anatomical landmark used for higher resolution imaging. In all cases, tracer-labeled parabrachiothalamic axons were found confined to the VPMpc borders extrapolated from corresponding coronal sections from the Paxinos Rat Atlas. Furthermore, the parabrachiothalamic projection site was in the ventral–lateral quadrant of these borders at each injection experiment. E and F correspond to −3.7 mm AP coordinates. bv = blood vessel. For other abbreviations, see list. Scale bar = 300 μm in A (applies to A–C); 600 μm in F (applies to D–G); 300 μm in J (applies to H–K).

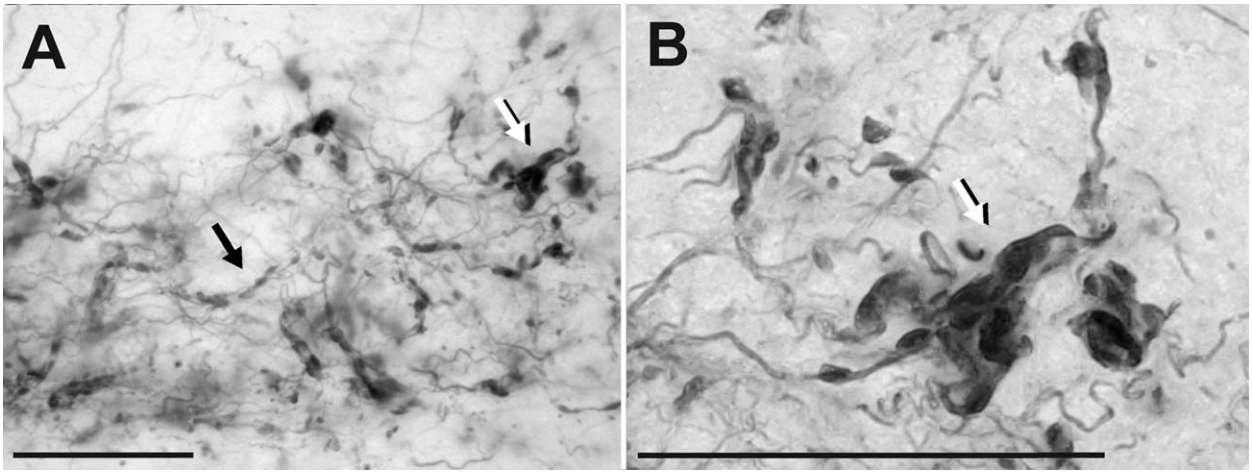

Figure 3. **A,B**. High-resolution images of anterogradely labeled parabrachiothalamic fibers displaying en passant swellings (black arrows) and large bouton-like structures (white arrows). Scale bar = 20 μm in A,B.

Consistent with prior studies that described the projection site of PBN neurons located in the waist region (Cechetto and Saper, 1987), the region containing dense anterograde labeling was within the medial portion of the VPMpc in all cases. Beyond providing landmarks for cell-sparse regions, Nissl-stained sections did not reveal any demarcations that matched the outlines provided in the Paxinos and Watson Atlas. However, myelin sections were useful in demarcating myelin-dense ventral (ml and arrows in Fig. 2J) and dorsal (arrowheads in Fig. 2J) landmarks. Neither the areas demarcated as the VPMpc in the Atlas, nor the myelination landmarks, provided a close-fitting envelope for the anterograde projection zone: the densely labeled region in the VPMpc was always surrounded by a projection-free zone, the outer borders of which matched dorsal and ventral myelination landmarks (Fig. 2J). An additional useful landmark was a large blood vessel that ran at the medial–ventral and dorsal–lateral axis, with several lateral bifurcations. The blood vessel was just medial to the dense anterogradely labeled region in the VPMpc in all cases examined (Fig. 2H–K, asterisks).

In most injection cases, DAB label was also sparsely present in areas outside of VPMpc borders that are demarcated by the myelination landmarks (Fig. 2H). Sparse fibers were also found in the contralateral hemisphere, in and around the VPMpc, but only the parabrachial fibers within the ipsilateral VPMpc were characterized further using the electron microscope. By using high-magnification objectives, we also observed that parabrachiothalamic projections within the VPMpc were comprised of a dense bundle of thick fibers with large swellings occurring along these labeled fibers (Fig. 3).

PBN tracer injections that produced dense anterograde labeling in the VPMpc also resulted in retrogradely filled cells in the rostral NTS, indicating accuracy of PBN injections (Fig. 4A–C). Tracer injections placed in the VPMpc and surrounding areas led to retrograde filling of cells in the PBN, but not in the NTS (Fig. 4D–L), confirming the lack of projections from the NTS to thalamus in the rat.

Electron microscopy

All brain sections that were processed for electron microscopy showed the same landmarks as those for light microscopy, including densely labeled fibers in the the VPMpc and myelinated axon bundles of the medial lemniscus. The ultrastructural morphology of labeled terminals and their postsynaptic targets within the parabrachiothalamic projection zone (Figs. 5–7) were examined systematically in four brains, and all labeled profiles encountered (i.e., all parabrachiothalamic axon segments regardless of whether they displayed a synapse at the cross section) were photographed at high resolution (10,000× magnification, 2.75 nm pixel size). Qualitatively, parabrachiothalamic terminals (labeled profiles that contain vesicles and a synapse) were large and formed multiple, punctate synapses. These terminals often wrapped around large-caliber dendrites that bore many dendritic protrusions. Many of these dendritic protrusions became immersed within a labeled bouton mass (Figs. 5A,B, 6A,B, 7C), and hence they can also be named “terminal inclusions.” Labeled boutons were invariably filled with vesicles and mitochondria. In lightly stained terminals, dense-core vesicles were detectable. The synapses formed by parabrachiothalamic terminals displayed postsynaptic densities of

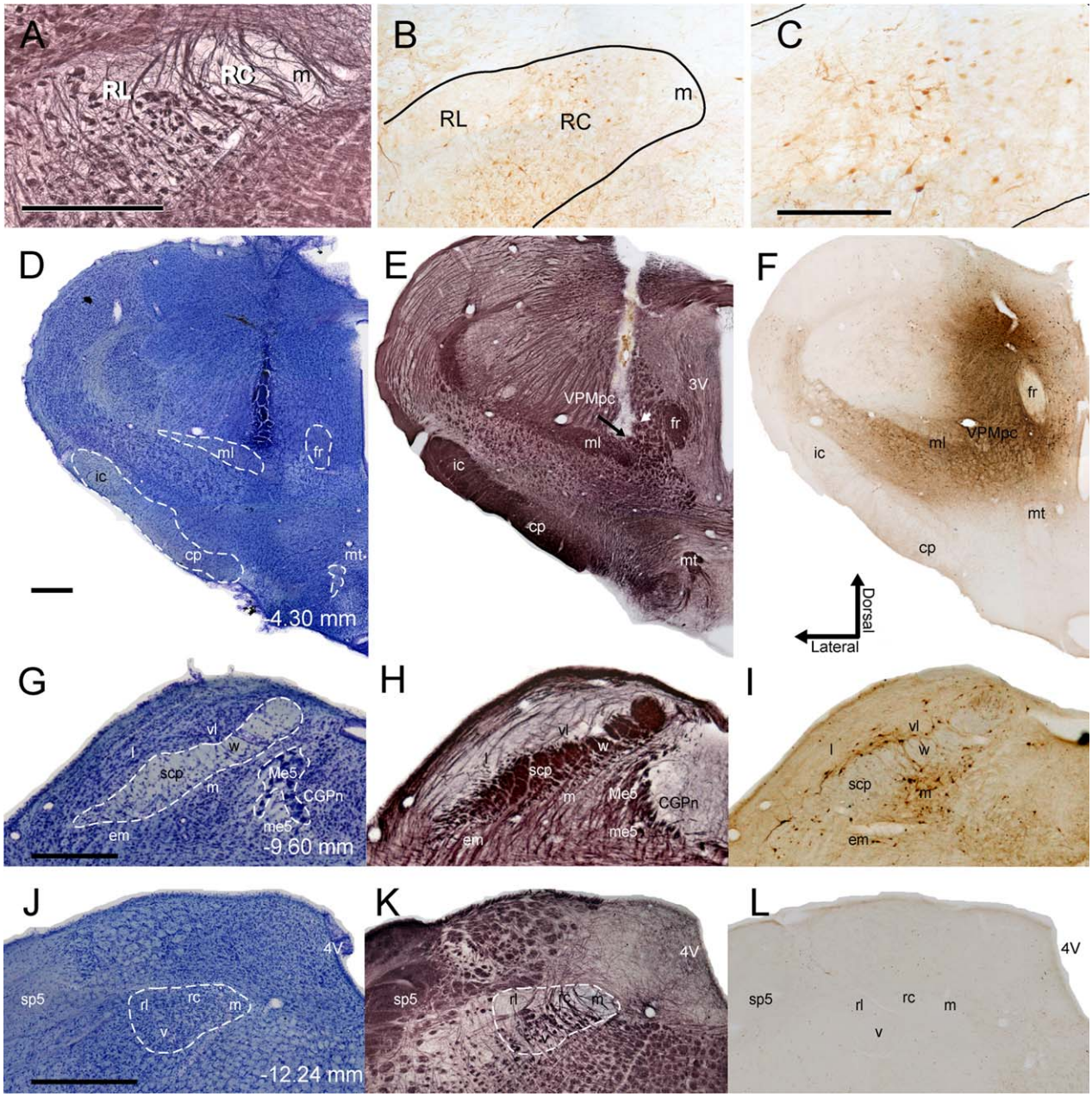

Figure 4. Retrograde transport of BDA after injections into the PBN (A–C) and VPMpc (D–L). Myelin (**A**) and the adjacent ABC/DAB (**B**) treated NTS sections after a tracer injection into the PBN waist region. NTS borders (determined from myelin stained sections) were transferred onto DAB-labeled sections. **C:** Higher magnification of section in B, illustrating retrogradely labeled neurons in the RC subdivision of the NTS. Nissl (**D**), myelin (**E**), and ABC/DAB (**F**) stained near-adjacent sections through the thalamus of a rat that received a large retrograde tracer injection into a region of the thalamus, including the VPMpc. Electrode tract is visible in D and E (black arrow in E), and the injection site in F. This injection resulted retrograde labeling in the PBN (**G–I**), including the waist region (w). However, no retrogradely labeled cells were encountered in the NTS (**J–L**). AP coordinate of the coronal sections corresponding to Nissl sample of each group is marked on the lower left corner of each Nissl section. NTS subdivisions: rl = rostrolateral, rc = rostrocentral, v = ventral, m = medial. sp5 = spinal trigeminal tract, 4V = fourth ventricle. For other abbreviations, see list. Scale bar = 150 μm in A (applies to A,B); 50 μm in C; 300 μm in D(applies to D–F); 300 μm in G (applies to G–I); 300 μm in J (applies to J–L).

varying thickness, whereas a mesh of electron-dense material was often present close to the postsynaptic density, giving an "underlined" appearance to the synaptic zone (Fig. 6A,B). Whereas a large area of the lipid bilayer membranes of labeled terminals and postsynaptic dendrites remained apposed to each other, synaptic zones that formed between these two elements were punctate. In 3D reconstructions, synaptic zones

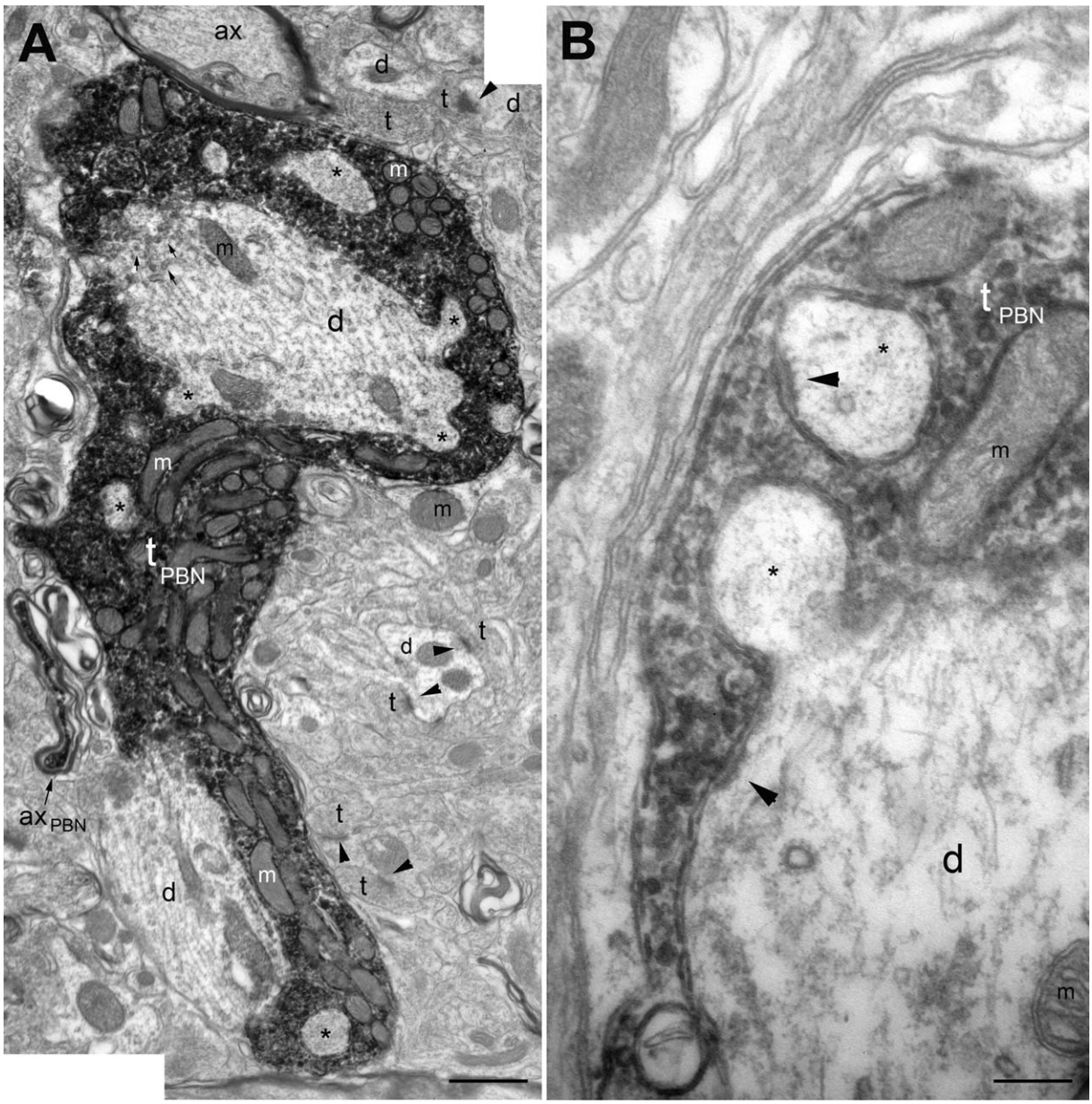

Figure 5. Electron micrographs of anterogradely labeled parabrachiothalamic terminals in the VPMpc. **A:** A large parabrachiothalamic terminal (t_{PBN}) almost completely surrounds a large-caliber dendrite (d), which contains somatic organelles (i.e., rER or ribosomes; small black arrows). Labeled axon segments are often myelinated (ax_{PBN}). Synapses formed by unlabeled terminals (t) onto small-caliber dendrites within the same field are marked with black arrowheads to aid in comparison of terminal and dendrite sizes. Postsynaptic dendrites extend protrusions (*) into the labeled terminal mass. **B:** Synaptic zones formed by labeled parabrachiothalamic terminals (black arrowhead) small in diameter, patchy and multiple. Postsynaptic dendrite protrusions (*) contain synaptic zones formed by the labeled terminals. m = mitochondria; ax = axon. For other abbreviations, see list. Scale bar = 1 μm in A; 0.25 μm in B.

appeared as patchy, elongated strips that extended along the axis of the dendrite (Fig. 7B). Dendritic protrusions (or unlabeled terminal inclusions) almost always contained a synaptic zone (Figs. 5B, 6A, 7C).

To quantify the morphological differences between parabrachiothalamic terminals and other inputs to the same region in the VPMpc, terminal cross-sectional areas of 98 labeled and 637 unlabeled terminals encountered within the same photographs were compared (Fig. 6D). Unlabeled terminal cross-sectional area was 0.35 ± 0.01 μm^2 on average (±SEM), with a range of 2.8 μm^2 (median 0.30 μm^2). In contrast, labeled terminals were 1.91 ± 0.31 μm^2 on average, with a range of 25.2 μm^2, and a median of 0.84 μm^2. The size difference between unlabeled and labeled terminal cross-sectional areas was statistically significant (Mann–

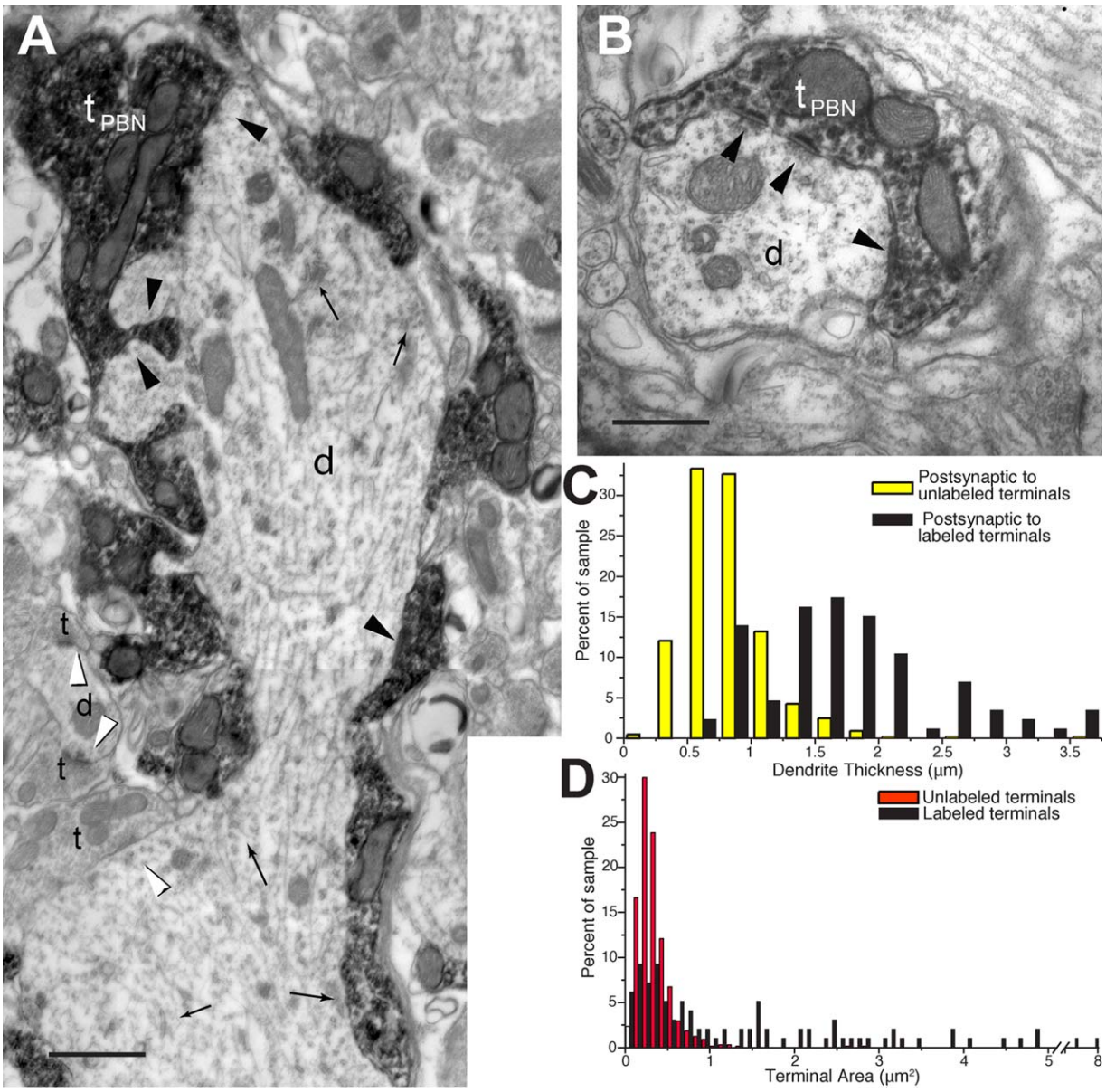

Figure 6. **A,B:** Anterogradely labeled parabrachiothalamic terminals (t_{PBN}) may also display smaller cross sections at the level of synaptic zones (black arrowheads). The presence of somatic organelles (small black arrows) indicates a proximal dendrite. Smaller caliber postsynaptic dendrites were also encountered (B). White arrowheads mark synapses formed by unlabeled terminals. **C:** Size-distribution histograms of dendrite caliber (measured as $feret_{min}$; see Materials and Methods for details) of dendrites postsynaptic to labeled parabrachiothalamic (black bars) versus dendrites that are postsynaptic unlabeled terminals (white bars) within the same regions as the labeled terminals. **D:** Cross-sectional area distribution histograms of labeled parabrachiothalamic terminals (black bars) versus unlabeled terminals (white bars) within the same regions as the labeled terminals. Note that the X-axis is truncated at around 8 μm^2 to illustrate the distribution of unlabeled terminal areas. For abbreviations, see list. Scale bar = 1 μm in A; 0.5 μm in B.

Whitney U test, $P < 0.001$). The sample population included several large, labeled profiles: a completely vesicle-filled, multiple synapse–forming terminal bouton 25.18 μm^2 in its cross-sectional area, another over 10 μm^2, and two others over 7.5 μm^2 in cross-sectional area. Over 70% of all labeled terminals were larger than the average of unlabeled terminals, and over 60% of labeled terminals were larger than the unlabeled terminal average area +1 SD. Only 2 of 637 unlabeled terminals were larger than the average labeled terminals, and only 3% of unlabeled terminals were larger than the median size of labeled terminals (0.84 μm^2). Because anterograde tracer injections are not expected to fill all axons projecting to the region and some contralateral

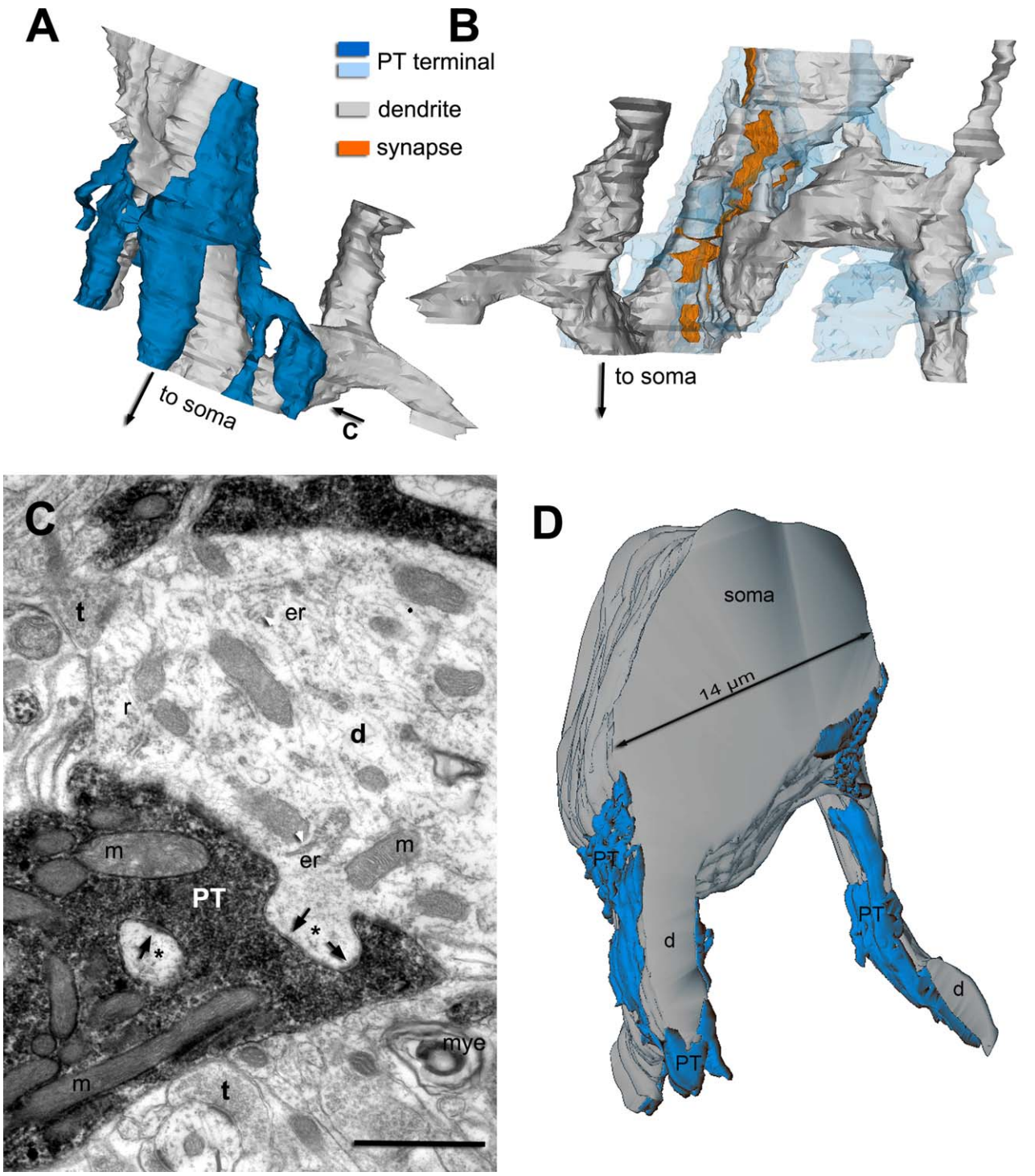

Figure 7. **A,B:** Three-dimensional reconstruction of a labeled parabrachiothalamic terminal (blue), making synapses (orange) onto a dendrite (gray). Small black arrows indicate the position of soma. **C:** Electron micrograph of sample planes (marked C and an arrow in A) of the reconstructed parabrachiothalamic terminal. Note that the synaptic zones from the labeled terminal are oriented parallel to the axis of the dendrite. **D:** 3D reconstruction of a VPMpc cell (blue) and anterogradely labeled parabrachiothalamic terminals (orange; PT) that extensively forms synapses onto the primary dendrite segments (d) of the cell. Abbreviations: m = mitochondrion; er = endoplasmic reticulum; r = ribosome; mye = myelin; t = terminal. Scale bar = 1 µm in C.

parabrachiothalamic projections exist, the large unlabeled terminals may in fact be parabrachiothalamic terminals. The striking size difference of parabrachiothalamic terminals from the rest of the VPMpc terminals suggests that size criterion alone is sufficient to identify parabrachiothalamic terminals.

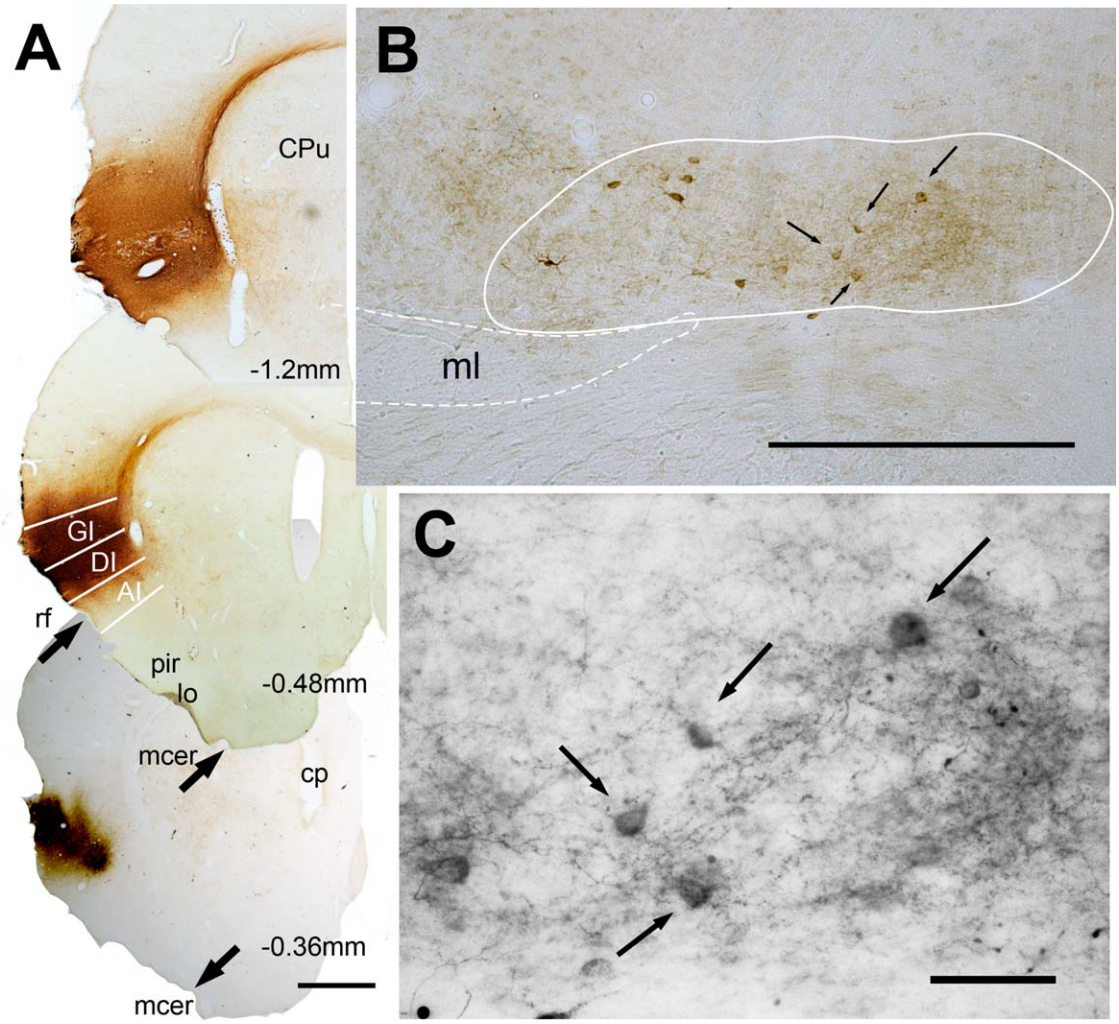

Figure 8. **A:** Insular cortex injection site from three animals. Approximate AP coronal positions of sections are matched to rat brain atlas (Paxinos and Watson, 1989), and marked at the lower corners of each section. Putative borders of the AI, DI, and GI were also transferred. All three injection sites included the putative DI and GI. **B:** Tracer labeling found in the VPMpc region after the bottom injection depicted in A. Both anterogradely filled fibers and retrogradely filled cells (arrows) in the VPMpc were found in the VPMpc. **C:** Higher magnification image of the region in the VPMpc containing retrogradely filled thalamocortical cells (arrows). Labeled fibers are fine and bear small swellings. Abbreviations: CPu = caudate putamen; cp = choroid plexus; rf = rhinal fissure; mcer = middle cerebral artery; pir = piriform cortex; lo = lateral olfactory tract. For other abbreviations, see list. Scale bar = 1 mm in A; 500 μm in B; 100 μm in C; 50 μm in D.

In quantifying the morphological properties of dendrites postsynaptic to labeled parabrachiothalamic terminals, we found that large-caliber dendrites are the main target of labeled terminals (Fig. 6C). The analyzed dataset included 86 dendrites postsynaptic to labeled terminals and 447 dendrites postsynaptic to unlabeled terminals. Dendrite cross sections that were not contained in their entirety within image frames, or those that did not display unambiguous borders, were not included in the analysis. Dendrites postsynaptic to labeled terminals were statistically larger than those postsynaptic to all other terminals (Mann–Whitney U test, $P < 0.001$). Labeled terminals were not the exclusive input to large dendrites. Although parabrachiothalamic terminals occupied an overwhelming area surrounding the dendrite, unlabeled terminals also synapsed with the same dendrite as the labeled parabrachiothalamic terminals (e.g., white arrowhead within postsynaptic dendrite in Fig. 6A).

The large diameter of dendrites postsynaptic to parabrachiothalamic terminals suggested that these might be proximal regions of the dendrites. In opportune sections, we were able to follow such postsynaptic dendrites into serially adjacent sections to confirm that the primary target of parabrachiothalamic terminals is proximal dendritic segments (Fig. 7). Furthermore, many postsynaptic dendrites contained perikaryal organelles (e.g., ribosomes and endoplasmic reticulum; Fig. 6A). Three-dimensional reconstruction also revealed that

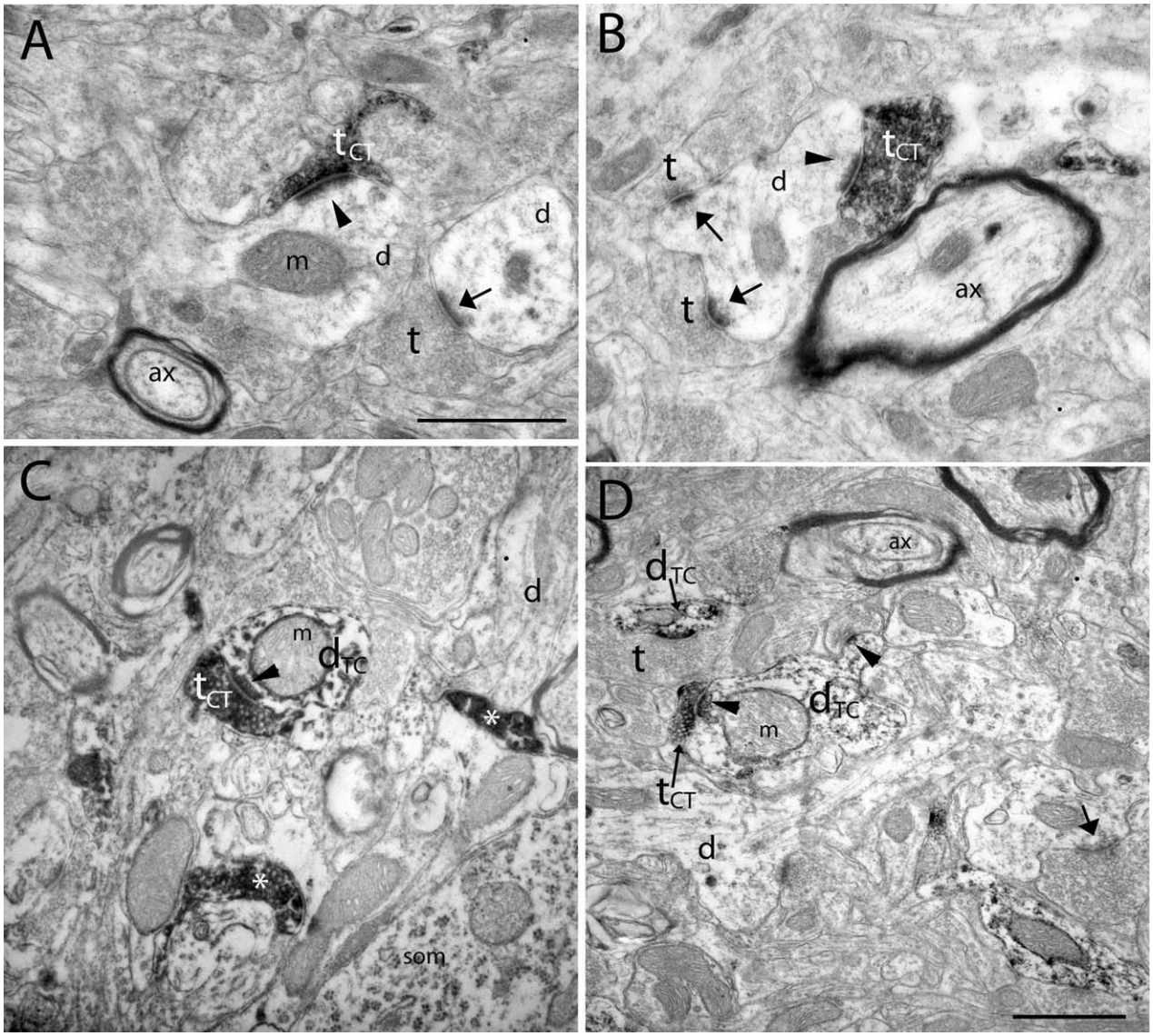

Figure 9. Electron micrographs of anterogradely filled corticothalamic terminals in the VPMpc. **A,B:** Anterogradely labeled corticothalamic terminals (t_{CT}) making synapses (arrowhead) onto small, unlabeled dendrites (d). **C,D:** Labeled corticothalamic terminals forming feedback synapses onto retrogradely labeled dendrites of thalamocortical neurons (d_{TC}). Other synapses (large arrows) made by unlabeled terminals (t) onto unlabeled dendrites are also shown in the graphs. Asterisks indicate an example of labeled corticothalamic terminals with no synaptic contact; such cross sections are not included in morphometric analyses. Abbreviations: m = mitochondria; ax = axon; som = soma. Scale bar = 1 μm in A (applies to A–C) and D.

large parabrachiothalamic boutons wrapped around the primary dendrites as the dendrites emerged from the somata, forming synaptic zones of massive total size between a single axon and the postsynaptic somata (Fig. 7B).

To quantify the frequency of parabrachiothalamic synapses in the VPMpc, we constructed composites of continuous areas from three brains, and examined an area of 6,016 μm^2 within the projection region. Within this restricted area we found 666 synaptic terminals, and only 13 of those contained BDA label. Thus, parabrachiothalamic terminals provided only 1.99% of all synaptic boutons in the VPMpc. However, even though the number of terminal boutons was small relative to all other inputs to the gustatory thalamus, parabrachiothalamic terminals, which form large and multiple synaptic zones onto their postsynaptic targets, provided 15% of the total surface area of synapse active zones in the thalamus circuitry, as measured by total synapse length of labeled and unlabeled terminals within the composite area dataset (28.5 μm synapse length from 13 parabrachiothalamic terminals versus 183.3 μm synapse length from 653 non-parabrachiothalamic terminals).

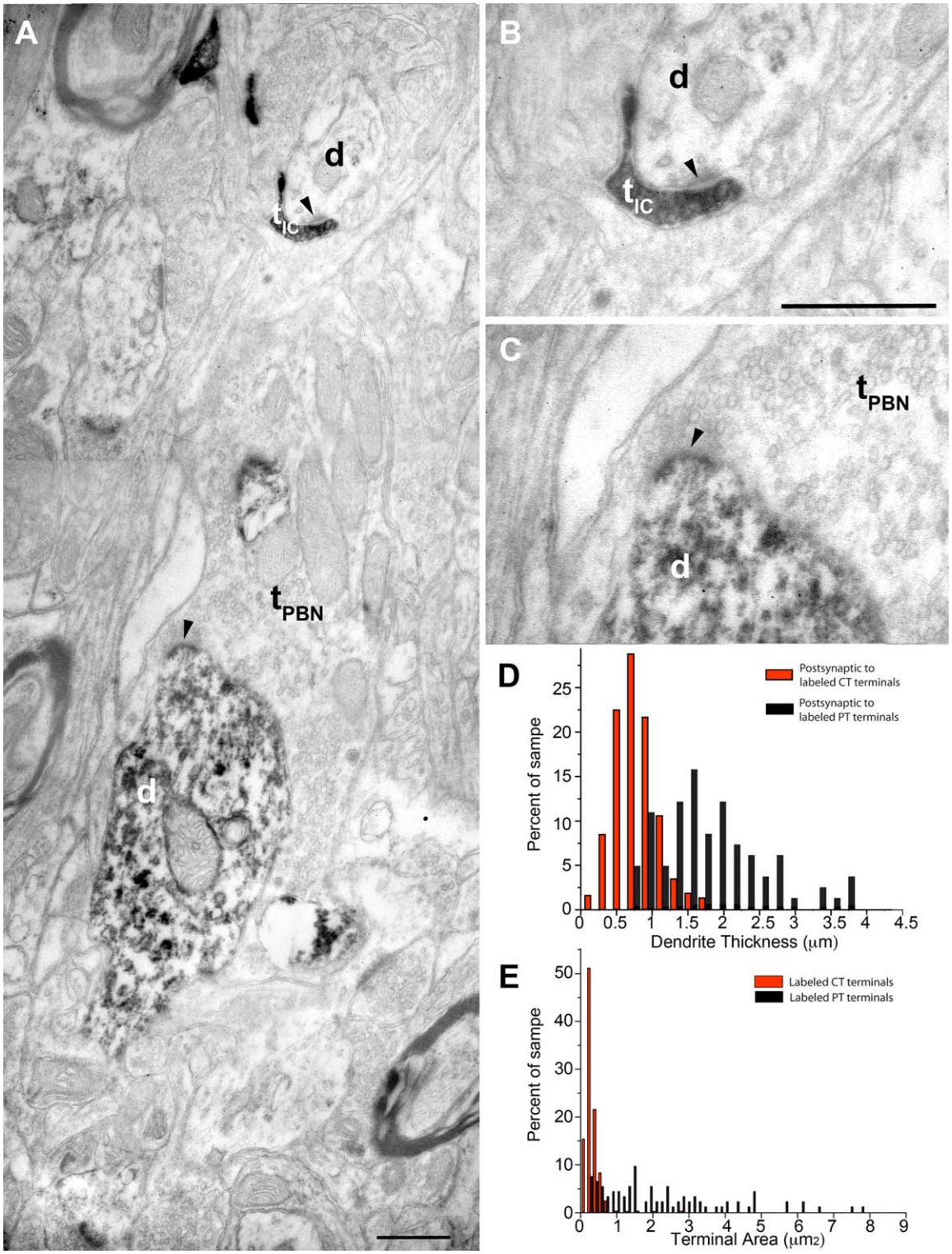

Figure 10. **A:** Composite electron micrographs in the VPMpc, showing an anterogradely labeled corticothalamic terminal (t_{IC}) that makes a synapse (arrowhead) onto a small, unlabeled dendrite (d). A large terminal (t_{PBN}) in the same field makes a synapse onto a retrogradely labeled dendrite (i.e., thalamocortical neuron). **B,C:** Higher magnification views of the synapses shown in A. **D:** Size distribution histograms of the calibers of dendrites that are postsynaptic to corticothalamic terminals (open bars) and parabrachiothalamic terminals (black bars). **E:** Size distribution histograms of cross-sectional areas of corticothalamic terminals (open bars) and parabrachiothalamic terminals (black bars). For abbreviations, see list. Scale bar = 500 nm in A; 500 nm in B (applies to B,C).

Corticothalamic input to the VPMpc

Anterograde tracer injections into the IC led to visualization of anterogradely filled fibers in the ipsilateral VPMpc (Fig. 8). A few retrogradely filled cells were also present within the VPMpc borders (Fig. 8B,C). This confirmed that injections included IC regions that were targeted by the VPMpc, and validated the presence of reciprocal connectivity between the VPMpc and IC. Serial sections of thalamus processed for DAB and myelin staining confirmed that there was a dense network of anterogradely labeled corticothalamic fibers, located in an ovoid area dorsal and medial to the medial lemniscus (Fig. 8B). Anterogradely filled corticothalamic fibers were fine and numerous and formed en passant swellings as well as short side arms terminating with a small bouton (Fig. 8C). Anterogradely filled boutons were also present in close proximity to retrogradely filled cell bodies.

Thalamic sections from three brains with tracer-visualized corticothalamic projections in the VPMpc were processed for electron microscopy. VPMpc landmarks and tracer label were confirmed by comparisons of myelin-stained series and Rat Brain Atlas maps with resin-embedded thick tissue sections under the light microscope. Resin-embedded blocks were trimmed to contain the medial VPMpc. In each brain, at least 2,700 μm^2 of tissue (total of 10,936 μm^2) was imaged and contained a total of 372 labeled terminals. The corticothalamic terminals were small, vesicle-dense, and characteristically lacked mitochondria (Fig. 9). Terminals formed single, asymmetric synaptic zones onto postsynaptic dendritic segments. Unlike parabrachiothalamic terminals, labeled corticothalamic terminals contained no dendritic protrusions (compare Figs. (5 and 6) and 9). Anterogradely labeled corticothalamic terminals were located in the same region as retrogradely filled VPMpc cells and dendrites. Synaptic connections between anterogradely and retrogradely labeled profiles were observed, suggesting that thalamic neurons that project to the IC receive direct synaptic feedback from the same region. Furthermore, retrogradely filled dendrites received synapses from large unlabeled terminal boutons (that is, from parabrachiothalamic terminals, identified by the size criterion), strongly suggesting that thalamocortical projection neurons receive monosynaptic parabrachiothalamic input. It should be noted that there are currently no VPMpc single-cell axon reconstructions in the literature. Therefore, it is not known whether thalamocortical axons give off axon collaterals within the VPMpc. If they do, these may also constitute a source of labeled terminal boutons found in the VPMpc after IC injections.

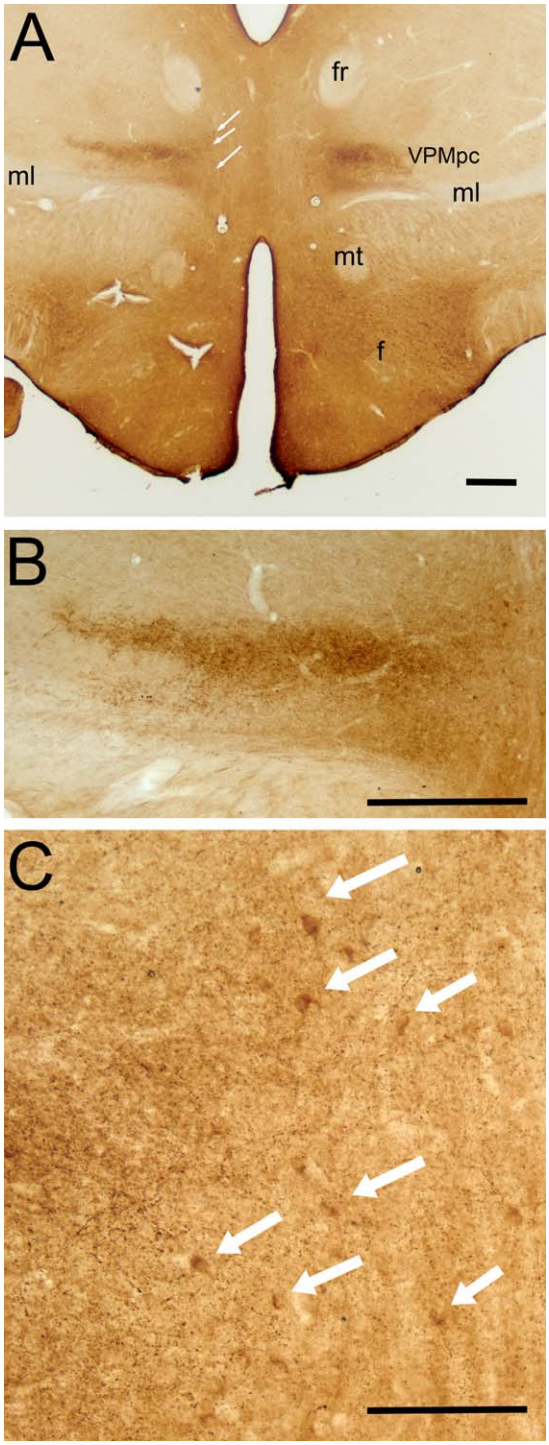

Figure 11. **A:** Immunolabeling with CGRP antibody leads to selectively dark labeling in the VPMpc. **B:** High-magnification examination reveals punctate, possibly terminal labeling. **C:** A few CGRP-labeled cells are observed medial to the VPMpc, in the A11 dopamine cell group (white arrows in A and C), as described before (Orazzo et al., 1993; Kresse et al., 1995). Note that the area of dense CGRP labeling in the VPMpc spreads dorsoventrally in the medial VPMpc, in contrast to parabrachiothalamic fibers from the waist region that we observed to be confined in a ventral position. For abbreviations, see list. Scale bar = 600 μm in A,B; 100 μm in C.

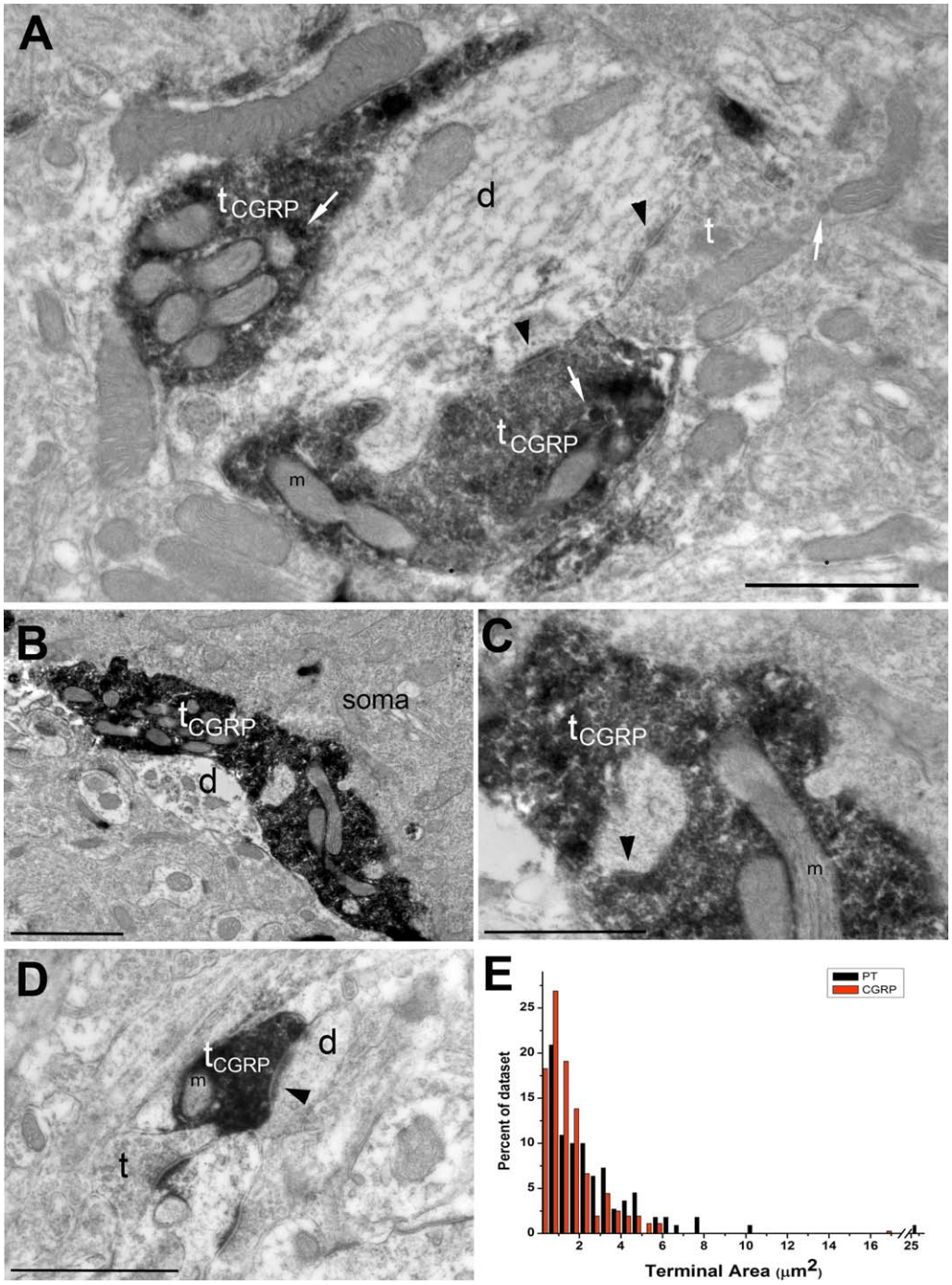

Figure 12. (A-D) Electron micrographs of CGRP-labeled terminals in the VPMpc, illustrating large (**A–C**) and small (**D**) CGRP-labeled terminals making synapses (arrowheads) onto postsynaptic dendrites (d). A soma is labeled in C showing close position to a labeled large CGRP terminal. The CGRP-DAB was often concentrated on dense-core vesicles (white arrows), yet not all terminals with dense-core vesicles were labeled with CGRP (white arrow in unlabeled terminal, t, in A). **E:** The comparison between area distribution histograms of CGRP (dashed line) and parabrachiothalamic (solid line) terminals. Scale bar = 1 μm in A,C,D; 2 μm in B.

The cross-sectional areas of corticothalamic terminals ($n = 372$) were significantly smaller than the parabrachiothalamic terminals (0.29 ± 0.22 μm^2 vs. 1.91 ± 3.1 μm^2; mean ± SD; Mann–Whitney U test, $P < 0.001$; Fig. 10). Corticothalamic terminals were also statistically smaller than the set of all non-parabrachiothalamic terminals (i.e., unlabeled terminals in parabrachiothalamic experiments; 0.29 ± 0.22 μm^2 vs. 0.35 ± 0.22 μm^2; Mann–Whitney U test, $P < 0.001$). Furthermore, we found that, unlike parabrachiothalamic terminals, the

primary target of corticothalamic terminals was small-caliber dendrites (0.74 ± 0.29 μm vs. 1.85 ± 0.90 μm, Mann–Whitney U test, $P < 0.001$). Dendrites that were retrogradely filled with tracer injected into the insular cortex were also postsynaptic to corticothalamic terminals. No axosomatic synapses were encountered between corticothalamic terminals and retrogradely filled VPMpc cells.

CGRP terminals in the VPMpc

A selective projection into the medial VPMpc carries CGRP (Yasui et al., 1989), and these projections are proposed to originate in the PBN (Dobolyi et al., 2005). Furthermore, the electron microscopic morphology of CGRP-positive fibers in the VPMpc (Williamson and Ralston, 1993) are qualitatively similar to the axons anterogradely filled from the waist region of the PBN in our study. To explore the possibility that CGRP immunolabeling could be used as a marker for parabrachiothalamic terminals in the VPMpc, we compared the morphometry of terminals labeled with CGRP immunolabeling or anterograde tracer labeling from the waist region of the PBN. The CGRP immunolabeling resulted in dense fiber staining in the regions dorsal and medial to the medial lemniscus (Fig. 11). CGRP fibers were particularly dense in the VPMpc, whereas CGRP-labeled cell bodies were noted in the dorsal subparafascicular thalamic nuclei and A11 dopaminergic cells, located just medial to the VPMpc (Fig. 11), confirming previous results characterizing CGRP labeling in the thalamus (Orazzo et al., 1993; Coolen et al., 2003). The medial and dorsal portions of the VPMpc contained relatively denser labeling. Under high-magnification light microscopy, CGRP-labeled fibers were seen to bear bouton-like swellings of various sizes. In general, CGRP-labeled fibers were fine with varicosities, and large fiber swellings, which resembled anterogradely labeled parabrachiothalamic fibers, were also observed.

In preparing CGRP-immunostained VPMpc sections for electron microscopy, the boundaries of the VPMpc were confirmed by comparing resin-embedded sections with adjacent Nissl- and myelin-stained sections, as described for tracer experiments. A total of 365 CGRP-labeled synaptic terminals within 16,586 μm^2 of imaged tissue were analyzed (Fig. 12). CGRP labeling filled vesicle-containing profiles in their entirety, although the label was particularly dense over dense-core vesicles (Fig. 12A, white arrows). As shown previously (Williamson and Ralston, 1993), there were at least two qualitatively different populations of CGRP terminals in the VPMpc. The first population was comprised of relatively large terminals filled with mitochondria and dense-core vesicles. Postsynaptic dendrites to these larger terminals were more likely to be large in diameter, and they enveloped dendritic protrusions that received synaptic input from those terminals (Fig. 12B,C). With these morphological characteristics, large CGRP terminals resembled anterogradely labeled parabrachiothalamic terminals (Fig. 12A–D, and compare with Fig. 5). However, not all terminals with parabrachiothalamic-like morphology were CGRP-positive. Large-caliber dendrites that received a synapse from CGRP-immunoreactive terminals also received other synapses from unlabeled, large, and dense-core vesicle-containing terminals (i.e., terminals that also display parabrachiothalamic terminal morphology; Fig. 12A). This indicates that CGRP may be present only in a subpopulation of parabrachiothalamic terminals. A second population consisted of smaller terminals (Fig. 11D) filled with vesicles and dense-core vesicles. These contained fewer, if any, mitochondria and usually synapsed on smaller caliber dendrites (Fig. 12D). No appendages or protrusion formations were observed at those dendrites postsynaptic to smaller CGRP terminals.

For quantitative comparison of CGRP terminals and anterogradely labeled parabrachiothalamic terminals in

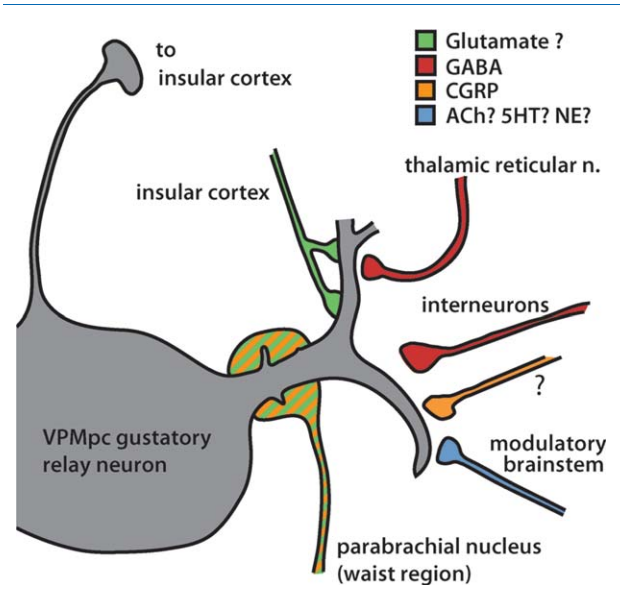

Figure 13. Summary illustration of inputs onto thalamocortical projection cells of the gustatory thalamic nucleus VPMpc. The parabrachiothalamic axons terminate on initial segments of primary dendrites via large boutons, which also contain CGRP. Feedback corticothalamic axons terminate on distal dendrites, via small terminals. Inhibitory synapses, presumably from local interneurons and thalamic reticular nucleus, also synapse on relay cells. Morphological selectivity of these inputs should be examined with specific markers. Whether the modulatory inputs from other brainstem nuclei, releasing acetylcholine, histamine, dopamine, or serotonin, are present in the VPMpc is not known. For abbreviations, see list.

the VPMpc, all labeled profiles that displayed a synapse at the cross section were measured. The average terminal area of all CGRP-immunoreactive terminals sampled was 1.51 ± 1.44 μm^2 (mean $\pm$ SD) with a range of 16.3 μm^2 (Fig. 12). Although the terminal area frequency histograms of CGRP-immunoreactive and parabrachiothalamic terminals were partially overlapping, statistical comparison revealed a significant difference between these populations of terminals (Mann–Whitney U test, $P < 0.001$). Furthermore, even though large terminals were present, only about 8% of all CGRP-labeled terminals were larger than the average size of non-parabrachiothalamic terminals. As outlined above, over 72% of all parabrachiothalamic terminals were larger than this same criterion. Thus, a great majority of CGRP terminals are more likely to be non-parabrachiothalamic, and CGRP immunoreactivity alone cannot be used as a marker for parabrachiothalamic terminals.

DISCUSSION

The current study examined the morphology and connectivity of two main inputs to the gustatory thalamus (VPMpc) in the rat: the primary input from the waist region of the PBN and the feedback projections from the insular cortex. The results demonstrated that parabrachiothalamic and corticothalamic inputs are morphologically distinct from each other, and they target different regions of dendrites (Fig. 13). Whereas parabrachiothalamic terminals are large, sparse, and highly selective for proximal dendritic segments of VPMpc relay cells, corticothalamic terminals are small and numerous and target distal dendrites. Morphometric properties suggest that size criterion alone is sufficient to reliably identify parabrachiothalamic terminals at the electron microscopic level. The results also provide evidence that although this peptide is not exclusive to parabrachiothalamic input originating from the waist region, CGRP is contained in a subset of parabrachiothalamic terminals.

Considerations on identification of the taste thalamus

The extent of the ipsilateral labeling observed in the gustatory thalamus is consistent with previous studies (Norgren and Leonard, 1973; Norgren, 1974, 1976), which documented brainstem projections by using lesion and tract-tracing approaches. Our results are also consistent with findings in studies that used anterograde (Karimnamazi and Travers, 1998; Bester et al., 1999) or retrograde (Krout and Loewy, 2000) tract tracing to indicate that the gustatory region of the the VPMpc is restricted to the medial portion. Cytoarchitectonic landmarks such as the fasciculus retroflexus, medial lemniscus, and mammilothalamic tract reliably mark the anterior–posterior zone along the VPMpc containing parabrachiothalamic input, although the actual borders of the VPMpc are ambiguous with Nissl or myelin stains. The borders drawn in the current study (Figs. 1, 2) are consistent with those drawn by Bester et al. (1999) and Paxinos and Watson (2007). Similar to our light microscopy observations, Bester et al. (1999) also pointed out that large varicosities of PBN projections clustering in a restricted pattern were found solely inside the VPMpc. These authors have also indicated that the PBN subnuclei that gave projections with those large varicosities were in the main parabrachial gustatory area, including the waist region and medial subnuclei. Despite our efforts with cytoarchitectonic or immunohistochemical markers, anterograde labeling from the waist region of the PBN remains the only unambiguous means to identify the projection site and the terminals of parabrachiothalamic axons.

Parabrachiothalamic input to the VPMpc

The VPMpc contains neurons that relay gustatory activity to the insular cortex. The present analysis of parabrachial terminal areas and postsynaptic dendrite caliber indicates that PBN projections provide a strong excitation on thalamic relay cells in the VPMpc, analogous to the role of primary, or driver, input axons observed in other primary sensory nuclei of the thalamus (e.g., the dorsal lateral geniculate nucleus, medial geniculate nucleus, and ventral posterior nucleus). Also characteristic of such driver inputs, parabrachiothalamic synapses constitute only a small proportion of all synapses in the VPMpc. In contrast, 3D reconstructions of the parabrachial terminals in the VPMpc demonstrated extensive interactions with the proximal dendrites of presumed relay cells in a pattern that is unmatched in any other primary sensory thalamic nuclei (Fig. 7). Although in visual, auditory, and somatosensory thalamic nuclei, principal sensory relay cells also receive their primary input at large-caliber, presumably proximal, dendrite segments (Liu et al., 1995; Erisir et al., 1998; Bartlett et al., 2000; Guillery and Sherman, 2002), highly exclusive and invasive targeting of initial dendrite segments of gustatory thalamic cells is unique to the gustatory system.

The functional implications of this innervation selectivity, and what it implies about the elaboration or the modulation of gustatory activity within the thalamus, are not immediately forthcoming. Thalamic relay cells in other sensory systems transmit sensory input to the cortex without much refinement in receptive field properties of their input cells or integration of multiple

sensory features, although many converging inputs from modulatory neurotransmitter systems may gate the transmission (Sherman, 2007). The axons from PBN neurons on VPMpc relay cells are situated to exert a strong excitation on individual neurons, possibly providing an excitatory signal capable of overwhelming other modulatory or integrated inputs. It is also worth noting that a major property of sensory thalamic nuclei, namely, glomerular arrangements and triads, are missing from the gustatory thalamus. The triads, commonly located within glomeruli, provide localized feedback inhibition to relay cells, and may mediate the timing of transmission in temporally sensitive, nonchemical sensory modalities (Sherman and Guillery, 2001; Saul, 2008). The present study demonstrated extensive synapse formation between large parabrachiothalamic terminal boutons and thalamocortical cells of the VPMpc. However, it is not known whether all parabrachiothalamic synapses on an individual relay cell belong to a single axon, or convergence of multiple parabrachiothalamic axons onto single relay cells occurs in the gustatory thalamus.

Corticothalamic input to the VPMpc

As shown previously, tracer injections centered in the insular cortex led to anterograde and retrograde labeling in the VPMpc (Nakashima et al., 2000; Lundy and Norgren, 2004). Anterogradely labeled axons formed synapses on retrogradely labeled dendrites, providing evidence for a corticothalamic feedback loop in the gustatory system. These corticothalamic terminals formed small boutons with asymmetric synapses, contacting distal dendrites of thalamic relay cells, which is also consistent with the glutamatergic feedback modulation that is encountered in all other sensory thalamic nuclei.

Accumulating evidence suggests that corticothalamic feedback in sensory thalamic nuclei may serve two main functions: enhancing receptive field properties of thalamocortical cells, and altering or strengthening the temporal patterns of activity in thalamic neuron ensembles (reviewed in Sillito and Jones, 2002; Briggs and Usrey, 2008). Relay cell receptive field refinement by corticothalamic activity has been reported for all nonchemical sensory systems (Sillito and Jones, 2002; Li and Ebner, 2007; Zhang and Yan, 2008), by which topographic organization of receptive fields can be selectively modified by discretely reciprocal projection patterns of corticothalamic axons. Anatomical projections from the insular cortex are as robust as in other sensory nuclei; however, the function of corticothalamic feedback in the gustatory thalamus is not forthcoming, especially because the gustatory neurons are broadly tuned and a topographic representation is not evident.

CGRP terminals in the VPMpc

Past studies have shown that the VPMpc is heavily innervated by CGRP-immunoreactive fibers, and the primary source of CGRP innervation is the ventral lateral, external medial, and external lateral region of the PBN (Yasui et al., 1991; Williamson and Ralston, 1993; de Lacalle and Saper, 2000; Dobolyi et al., 2005). In particular, using retrograde tracer injections that included the VPMpc in the thalamus, Yasui et al. (1989) have demonstrated that whereas many retrogradely labeled cells in visceral sensory divisions of the PBN contained CGRP, a small number of waist region neurons have also contained this peptide. These authors also provided evidence that CGRP-immunoreactive neurons in the external medial parabrachial subnucleus sent fibers prominently to the contralateral VPMpc region. In the present study, comparing ultrastructural morphological properties of CGRP-immunoreactive terminals in the VPMpc with anterogradely labeled parabrachiothalamic terminals, we documented the similarities between a subpopulation of CGRP-immunoreactive terminals and parabrachiothalamic terminals, namely, large boutons containing dense-core vesicles. Furthermore, we have noted that not all CGRP-immunoreactive terminals in the VPMpc displayed parabrachiothalamic morphology, and not all parabrachiothalamic terminals (as defined by a size criterion) contained CGRP. In addition to eliminating the possibility of using CGRP as a marker for PBN–waist region inputs to the VPMpc, these observations have two important implications.

First, PBN–waist region inputs to the VPMpc are not molecularly uniform; there are at least two separate subpopulations, each with a different chemical phenotype, even though they may be morphologically uniform. The functional significance of CGRP in these chemical sensory axons is not known.

Second, given that the origin of small CGRP terminals is not ipsilateral PBN–waist projections (current findings), and that the brainstem is the most likely source of all CGRP labeling in the VPMpc (because transections at superior cerebral peduncle eliminate all CGRP labeling in fibers located in the VPMpc; Dobolyi et al., 2005), the external medial parabrachial nucleus, which projects to the contralateral VPMpc, may in fact be the origin of the small CGRP-immunoreactive terminals there. In the current study we have not targeted external medial subdivisions for our injections, nor did we analyze contralateral projections. Future studies should confirm that contralateral parabrachiothalamic axons, which may bring the visceral sensory information to the VPMpc, are morphologically distinct from ipsilateral, pontine taste axons.

The possibility that gustatory information is modulated by visceral sensory input in rats, as well as in

primates, was suggested previously (Yasui et al., 1989; de Lacalle and Saper, 2000). Our findings provide inferential support for this idea, by demonstrating the anatomical evidence for a substantial CGRP input that originates from nontaste subdivisions of the parabrachial nucleus. Studying the functional role of CGRP/glutamate co-release in the VPMpc will add to our understanding of intrinsic modulation of sensory processing in the gustatory thalamus.

Functional implications for the VPMpc circuitry

Response properties of VPMpc neurons have been characterized in a few studies (Scott and Erickson, 1971; Scott and Yalowitz, 1978; Nomura and Ogawa, 1985; Ogawa and Nomura, 1988; Verhagen et al., 2003). The presence of three major neuron types, which closely mimic the physiological types encountered in the NTS, were proposed: NaCl-, HCl-, and sucrose-oriented neurons (Verhagen et al., 2003). A small population of quinine-oriented neurons was also encountered. Response properties of VPMpc cells are consistent with the role of the VPMpc as a relay nucleus of taste information: similar to gustatory responses in NTS and PBN cells, VPMpc neurons are broadly tuned, yet tastant-selective (Verhagen et al., 2005). Consistent with the idea of existence of functional neuron types at this relay, neuron groups with selectivity to different tastants respond to selective sodium blocks applied in the oral cavity, similar to those in the NTS and PBN (Verhagen et al., 2005). Furthermore, the breadth of VPMpc cell tastants-tuning and their overall spontaneous firing rates are intermediate between NTS and cortex cell response patterns. Thalamocortical cells are better able to differentiate tastants than the neurons in the lower gustatory nuclei (Scott and Erickson, 1971), indicating that sharpening of gustatory receptive fields may occur via thalamic gustatory processing.

This suggests that some aspects of the tuning properties are refined as taste information is transmitted along the thalamocortical pathway, perhaps utilizing the temporal information to distinguish responses of broadly tuned neurons for stimuli in the same category (Verhagen et al., 2003; Carleton et al., 2010). The synaptic selectivity of parabrachiothalamic axons revealed in the current study also indicates that individual brainstem axons may be sufficient to drive spiking activity in relay neurons. There are no reports available to indicate anatomical phenotypes of neurons in correlation with their response selectivity, nor to identify synaptic connectivity patterns of axons that preserve distinct stimulus properties along the NTS–PBN–VPMpc axis. Our results implying at least two distinct populations of PBN axons in the VPMpc (those that do and do not contain CGRP) may be indicative of a structural basis for differential synaptic circuitry involving functional neuron types in the VPMpc.

Chemical versus nonchemical thalamus

Sensory pathways in mammals follow a well-described hierarchical pattern: Each specific sensory input arrives to corresponding primary cortical area via a thalamic relay nucleus, which is defined as the *first-order relay* (Sherman, 2007). The primary cortical area, in turn, projects to a *higher order thalamic relay* nucleus, which is the source of the primary (or driver) input to secondary sensory cortical areas. The driver inputs to both the first-order and the higher order thalamic relay nuclei are distinguished by a long list of features, including thick axons bearing large terminal boutons and providing a surprisingly small percentage of the synapses on relay cells, the type of glutamate receptors (only ionotropic), and the provision of receptive field properties maintained in the receptor organ or the specific brainstem nuclei. Even though light microcopy studies have demonstrated that parabrachiothalamic axons project densely to the VPMpc and bear large swellings (Bester et al., 1999), and have indicated that the basic connectivity of gustatory thalamic relay may fit the general pattern of all other first-order sensory thalamic nuclei, many questions have remained regarding their synaptic properties, which could only be answered at ultrastructural resolution.

The current study examined the ultrastructure of the VPMpc with respect to its main ascending input from the PBN, and its main feedback projection from the insular cortex in the adult rat, and revealed the similarities, and unique properties, of gustatory thalamic circuitry with other first-order thalamic relay nuclei. First, the demonstration that parabrachiothalamic terminal boutons are sparse, and that they constitute the largest terminal boutons in the taste thalamus, confirms that the VPMpc fits the definition of first-order thalamic relay nucleus. Whether there is a higher order thalamic relay for the taste system remains unknown.

Second, morphological properties of parabrachiothalamic axons leave no ambiguity in that this input should be sufficient to drive the excitation that will be relayed to the IC, in a manner analogous to primary “driver” inputs to visual, auditory, and somatosensory thalamic nuclei. Corticothalamic input morphology and targeting properties are also in agreement with known patterns of innervation of sensory thalamic nuclei. However, a hallmark structural component of these nonchemical thalamic nuclei is missing from the VPMpc; glomerular

structures, that is, glia-encapsulated triadic arrangements among primary and inhibitory axons and relay cell dendrites, are not encountered in the VPMpc. In contrast, glomerular arrangements are common in the NTS (May et al., 2007; Wang et al., 2012), suggesting that at least some of the specialized processing attributed to nonchemical thalamic nuclei circuitry may take place in brainstem nuclei in taste pathways.

Lastly, we would like to point out the possibility that the similarities and unique properties of VPMpc circuitry unveiled in the current study may be peculiar to rodent species. As has been documented in detail (Beckstead et al., 1980; Pritchard et al., 2000; Lundy and Norgren, 2004), the parabrachiothalamic input to the VPMpc replaces the direct input from the NTS that is found in primates. This evolutionary divergence is unique not only in considering rodents versus primates, but also in considering chemical versus nonchemical senses in rodents. That is, unlike the rodent taste system, brainstem-to-thalamus pathways persist in rodent auditory and somatosensory systems. Therefore, the morphological properties of parabrachiothalamic axons and the VPMpc circuitry we have demonstrated in the current study may be unique to rodents as well. Examination of primate thalamus morphology and circuitry may allow direct comparisons of chemical and nonchemical thalamic circuitries and function in primates, including humans.

CONCLUSIONS

The current study is a first step in understanding the structural organization of inputs to neurons in the gustatory thalamus, and thus the anatomical basis for gustatory processing along the brainstem–thalamus–cortex pathway. It also underlines the unique properties of gustatory thalamus synaptic organization in comparison with other sensory pathways in rodents.

ACKNOWLEDGMENTS

The authors thank Bonnie Sheppard for technical expertise in electron microscopy serial sectioning.

CONFLICT OF INTEREST STATEMENT

The authors have no conflicts of interest.

ROLE OF AUTHORS

All authors had full access to all the data in the study; they take responsibility for the integrity of the data and the accuracy of the data analysis. The contributions of each author are as follows:

Study concept and design: JAC, AE. Acquisition of data: SLH, AF, WF, AE. Analysis and interpretation of data: SLH, JAC, AF, AE. Drafting of the manuscript: SLH, AF, JAC, AE. Critical revision of the manuscript: SLH, AF, JAC, AE. Obtained funding: AE, SLH, JAC. Study supervision: AE.

LITERATURE CITED

Allen GV, Saper CB, Hurley KM, Cechetto DF. 1991. Organization of visceral and limbic connections in the insular cortex of the rat. J Comp Neurol 311:1–16.

Bartlett EL, Stark JM, Guillery RW, Smith PH. 2000. Comparison of the fine structure of cortical and collicular terminals in the rat medial geniculate body. Neuroscience 100:811–828.

Beckstead RM, Morse JR, Norgren R. 1980. The nucleus of the solitary tract in the monkey: projections to the thalamus and brain stem nuclei. J Comp Neurol 190:259–282.

Benjamin RM, Akert K. 1959. Cortical and thalamic areas involved in taste discrimination in the albino rat. J Comp Neurol 111:231–259.

Bester H, Bourgeais L, Villanueva L, Besson JM, Bernard JF. 1999. Differential projections to the intralaminar and gustatory thalamus from the parabrachial area: a PHA-L study in the rat. J Comp Neurol 405:421–449.

Blum M, Walker AE, Ruch TC. 1943. Localization of taste in the thalamus of *Macaca mulatta*. Yale J Biol Med 16: 175–192.1.

Briggs F, Usrey WM. 2008. Emerging views of corticothalamic function. Curr Opin Neurobiol 18:403–407.

Carleton A, Accolla R, Simon SA. 2010. Coding in the mammalian gustatory system. Trends Neurosci 33:326–334.

Cechetto DF, Saper CB. 1987. Evidence for a viscerotopic sensory representation in the cortex and thalamus in the rat. J Comp Neurol 262:27–45.

Coolen LM, Veening JG, Petersen DW, Shipley MT. 2003. Parvocellular subparafascicular thalamic nucleus in the rat: anatomical and functional compartmentalization. J Comp Neurol 463:117–131.

Corson JA, Aldridge A, Wilmoth K, Erisir A. 2012. A survey of oral cavity afferents to the rat nucleus tractus solitarii. J Comp Neurol 520:495–527.

de Lacalle S, Saper CB. 2000. Calcitonin gene-related peptide-like immunoreactivity marks putative visceral sensory pathways in human brain. Neuroscience 100:115–130.

Dobolyi A, Irwin S, Makara G, Usdin TB, Palkovits M. 2005. Calcitonin gene-related peptide-containing pathways in the rat forebrain. J Comp Neurol 489:92–119.

Emmers R. 1964. Localization of thalamic projection of afferents from the tongue in the cat. Anat Rec 148:67–74.

Erisir A, Van Horn SC, Sherman SM. 1998. Distribution of synapses in the lateral geniculate nucleus of the cat: differences between laminae A and A1 and between relay cells and interneurons. J Comp Neurol 390:247–255.

Fiala JC. 2005. Reconstruct: a free editor for serial section microscopy. J Microsc 218:52–61.

Guillery RW, Sherman SM. 2002. Thalamic relay functions and their role in corticocortical communication: generalizations from the visual system. Neuron 33:163–175.

Halsell CB, Travers SP. 1997. Anterior and posterior oral cavity responsive neurons are differentially distributed among parabrachial subnuclei in rat. J Neurophysiol 78: 920–938.

Hamilton RB, Norgren R. 1984. Central projections of gustatory nerves in the rat. J Comp Neurol 222:560–577.

Hanamori T. 2003. Chemical stimulation of the thalamic reticular nucleus inhibits the neuronal activity of the posterior insular cortex in rats. Chem Senses 28:717–728.

Hayama T, Hashimoto K, Ogawa H. 1994. Anatomical location of a taste-related region in the thalamic reticular nucleus in rats. Neurosci Res 18:291–299.

Herbert H, Moga MM, Saper CB. 1990. Connections of the parabrachial nucleus with the nucleus of the solitary tract and the medullary reticular formation in the rat. J Comp Neurol 293:540–580.

Karimnamazi H, Travers JB. 1998. Differential projections from gustatory responsive regions of the parabrachial nucleus to the medulla and forebrain. Brain Res 813:283–302.

Katz DB, Simon SA, Nicolelis MA. 2001. Dynamic and multimodal responses of gustatory cortical neurons in awake rats. J Neurosci 21:4478–4489.

Kosar E, Grill HJ, Norgren R. 1986a. Gustatory cortex in the rat. II. Thalamocortical projections. Brain Res 379:342–352.

Kosar E, Grill HJ, Norgren R. 1986b. Gustatory cortex in the rat. I. Physiological properties and cytoarchitecture. Brain Res 379:329–341.

Kresse A, Jacobowitz DM, Skofitsch G. 1995. Detailed mapping of CGRP mRNA expression in the rat central nervous system: comparison with previous immunocytochemical findings. Brain Res Bull 36:261–274.

Krout KE, Loewy AD. 2000. Parabrachial nucleus projections to midline and intralaminar thalamic nuclei of the rat. J Comp Neurol 428:475–494.

Lasiter PS, Kachele DL. 1988. Postnatal development of the parabrachial gustatory zone in rat: dendritic morphology and mitochondrial enzyme activity. Brain Res Bull 21:79–94.

Li L, Ebner FF. 2007. Cortical modulation of spatial and angular tuning maps in the rat thalamus. J Neurosci 27:167–179.

Liu XB, Honda CN, Jones EG. 1995. Distribution of four types of synapse on physiologically identified relay neurons in the ventral posterior thalamic nucleus of the cat. J Comp Neurol 352:69–91.

Lundy RF, Norgren R. 2004. Gustatory system. In: Paxinos G, editor. The rat nervous system, 3rd ed. San Diego, CA: Academic Press. p 890–921.

Malpeli JG. 1983. Activity of cells in area 17 of the cat in absence of input from layer a of lateral geniculate nucleus. J Neurophysiol 49:595–610.

May OL, Erisir A, Hill DL. 2007. Ultrastructure of primary afferent terminals and synapses in the rat nucleus of the solitary tract: comparison among the greater superficial petrosal, chorda tympani, and glossopharyngeal nerves. J Comp Neurol 502:1066–1078.

Nakashima M, Uemura M, Yasui Y, Ozaki HS, Tabata S, Taen A. 2000. An anterograde and retrograde tract-tracing study on the projections from the thalamic gustatory area in the rat: distribution of neurons projecting to the insular cortex and amygdaloid complex. Neurosci Res 36:297–309.

Nomura T, Ogawa H. 1985. The taste and mechanical response properties of neurons in the parvicellular part of the thalamic posteromedial ventral nucleus of the rat. Neurosci Res 3:91–105.

Norgren R. 1974. Gustatory afferents to ventral forebrain. Brain Res 81:285–295.

Norgren R. 1976. Taste pathways to hypothalamus and amygdala. J Comp Neurol 166:17–30.

Norgren R, Leonard CM. 1971. Taste pathways in rat brainstem. Science 173:1136–1139.

Norgren R, Leonard CM. 1973. Ascending central gustatory pathways. J Comp Neurol 150:217–237.

Norgren R, Wolf G. 1975. Projections of thalamic gustatory and lingual areas in the rat. Brain Res 92:123–129.

Ogawa H, Nomura T. 1988. Receptive field properties of thalamo-cortical taste relay neurons in the parvicellular part of the posteromedial ventral nucleus in rats. Exp Brain Res 73:364–370.

Orazzo C, Pieribone VA, Ceccatelli S, Terenius L, Hökfelt T. 1993. CGRP-like immunoreactivity in A11 dopamine neurons projecting to the spinal cord and a note on CGRP-CCK cross-reactivity. Brain Res 600:39–48.

Paxinos G, Watson C. 2007. The rat brain in stereotaxic coordinates. San Diego, CA: Academic Press.

Piette CE, Baez-Santiago MA, Reid EE, Katz DB, Moran A. 2012. Inactivation of basolateral amygdala specifically eliminates palatability-related information in cortical sensory responses. J Neurosci 32:9981–9991.

Poulet JFA, Fernandez LMJ, Crochet S, Petersen CCH. 2012. Thalamic control of cortical states. Nat Neurosci 15:370–372.

Pritchard TC, Hamilton RB, Morse JR, Norgren R. 1986. Projections of thalamic gustatory and lingual areas in the monkey, *Macaca fascicularis*. J Comp Neurol 244:213–228.

Pritchard TC, Hamilton RB, Norgren R. 2000. Projections of the parabrachial nucleus in the Old World monkey. Exp Neurol 165:101–117.

Reiner A, Veenman CL, Medina L, Jiao Y, Del Mar N, Honig MG. 2000. Pathway tracing using biotinylated dextran amines. J Neurosci Methods 103:23–37.

Samuelsen CL, Gardner MPH, Fontanini A. 2012. Effects of cue-triggered expectation on cortical processing of taste. Neuron 74:410–422.

Samuelsen CLC, Gardner MPHM, Fontanini A. 2013. Thalamic contribution to cortical processing of taste and expectation. J Neurosci 33:1815–1827.

Saul AB. 2008. Lagged cells in alert monkey lateral geniculate nucleus. Vis Neurosci 25:647–659.

Scott TR, Erickson RP. 1971. Synaptic processing of taste-quality information in thalamus of the rat. J Neurophysiol 34:868–883.

Scott TR, Yalowitz MS. 1978. Thalamic taste responses to changing stimulus concentration. Chem Senses 3:167–175.

Sewards TV. 2004. Dual separate pathways for sensory and hedonic aspects of taste. Brain Res Bull 62:271–283.

Sherman SM. 2007. The thalamus is more than just a relay. Curr Opin Neurobiol 17:417–422.

Sherman SM, Guillery RW. 2001. Exploring the thalamus. San Diego, CA: Academic Press.

Sillito AM, Jones HE. 2002. Corticothalamic interactions in the transfer of visual information. Philos Trans R Soc Lond B Biol Sci 357:1739–1752.

Spector AC, Travers SP. 2005. The representation of taste quality in the mammalian nervous system. Behav Cogn Neurosci Rev 4:143–191.

Stapleton JR, Lavine ML, Wolpert RL, Nicolelis MAL, Simon SA. 2006. Rapid taste responses in the gustatory cortex during licking. J Neurosci 26:4126–4138.

Stehberg J, Acuña-Goycolea C, Ceric F, Torrealba F. 2001. The visceral sector of the thalamic reticular nucleus in the rat. Neuroscience 106:745–755.

Tokita K, Inoue T, Boughter JD Jr. 2010. Subnuclear organization of parabrachial efferents to the thalamus, amygdala and lateral hypothalamus in C57BL/6J mice: a quantitative retrograde double labeling. Neuroscience 171:351–365.

Verhagen JV, Giza BK, Scott TR. 2003. Responses to taste stimulation in the ventroposteromedial nucleus of the thalamus in rats. J Neurophysiol 89:265–275.

Verhagen JV, Giza BK, Scott TR. 2005. Effect of amiloride on gustatory responses in the ventroposteromedial nucleus of the thalamus in rats. J Neurophysiol 93:157–166.

Wang S, Corson JA, Hill DL, Erisir A. 2012. Postnatal development of chorda tympani axons in the rat nucleus of the solitary tract. J Comp Neurol 520:3217–3235.

Williamson AM, Ralston HJ. 1993. Fine structure of calcitonin gene-related peptide immunoreactive synaptic contacts in the thalamus of the rat. J Comp Neurol 328:130–144.

Wong HC, Taché Y, Lloyd KC, Yang H, Sternini C, Holzer P, Walsh JH. 2014. Monoclonal antibody to rat alpha-CGRP: production, characterization, and in vivo immunoneutralization activity. Hybridoma 12:93–106.

Yasui Y, Saper CB, Cechetto DF. 1989. Calcitonin gene-related peptide immunoreactivity in the visceral sensory cortex, thalamus, and related pathways in the rat. J Comp Neurol 290:487–501.

Yasui Y, Saper CB, Cechetto DF. 1991. Calcitonin gene-related peptide (CGRP) immunoreactive projections from the thalamus to the striatum and amygdala in the rat. J Comp Neurol 308:293–310.

Zhang L, Hoff AO, Wimalawansa SJ, Cote GJ, Gagel RF, Westlund KN. 2001. Arthritic calcitonin/alpha calcitonin gene-related peptide knockout mice have reduced nociceptive hypersensitivity. Pain 89:265–273.

Zhang Y, Yan J. 2008. Corticothalamic feedback for sound-specific plasticity of auditory thalamic neurons elicited by tones paired with basal forebrain stimulation. Cereb Cortex 18:1521–1528.